

A METHOD FOR THE DESIGN OF FRC TUNNEL LININGS REINFORCED  
WITH FRP BARS

A THESIS SUBMITTED TO  
THE GRADUATE SCHOOL OF NATURAL AND APPLIED SCIENCES  
OF  
MIDDLE EAST TECHNICAL UNIVERSITY

BY

MUTLU DEMİR

IN PARTIAL FULFILLMENT OF THE REQUIREMENTS  
FOR  
THE DEGREE OF MASTER OF SCIENCE  
IN  
CIVIL ENGINEERING

SEPTEMBER 2019



Approval of the thesis:

**A METHOD FOR THE DESIGN OF FRC TUNNEL LININGS  
REINFORCED WITH FRP BARS**

submitted by **MUTLU DEMİR** in partial fulfillment of the requirements for the degree of **Master of Science in Civil Engineering Department, Middle East Technical University** by,

Prof. Dr. Halil Kalıpçılar  
Dean, Graduate School of **Natural and Applied Sciences**

\_\_\_\_\_

Prof. Dr. Ahmet Türer  
Head of Department, **Civil Engineering**

\_\_\_\_\_

Prof. Dr. Uğurhan Akyüz  
Supervisor, **Civil Engineering, METU**

\_\_\_\_\_

**Examining Committee Members:**

Prof. Dr. Erdem Canbay  
Civil Engineering, METU

\_\_\_\_\_

Prof. Dr. Uğurhan Akyüz  
Civil Engineering, METU

\_\_\_\_\_

Prof. Dr. İsmail Özgür Yaman  
Civil Engineering, METU

\_\_\_\_\_

Assoc. Prof. Dr. Burcu Burak Bakır  
Civil Engineering, METU

\_\_\_\_\_

Assoc. Prof. Dr. Alper Aldemir  
Civil Engineering, Hacettepe University

\_\_\_\_\_

Date: 09.09.2019

**I hereby declare that all information in this document has been obtained and presented in accordance with academic rules and ethical conduct. I also declare that, as required by these rules and conduct, I have fully cited and referenced all material and results that are not original to this work.**

Name, Surname: Mutlu Demir

Signature:

## **ABSTRACT**

### **A METHOD FOR THE DESIGN OF FRC TUNNEL LININGS REINFORCED WITH FRP BARS**

Demir, Mutlu  
Master of Science, Civil Engineering  
Supervisor: Prof. Dr. Uğurhan Akyüz

September 2019, 77 pages

There are some difficulties in the construction of precast conventional reinforced concrete tunnel segments. Due to corrosion problem of ordinary reinforcement, the task becomes more complicated. Moreover, the workmanship for the construction of segments is also very time consuming. There are some research for the design of tunnel segments with fiber reinforced polymer (FRP) bars. Besides, guidelines for the design of fiber reinforced concrete (FRC) tunnel linings are also available.

This thesis provides a methodology for the design of FRC tunnel linings reinforced with FRP bars. The methodology is mainly based on the recommendations and limitations in accordance with fib Model Code 2010 (2012), bulletin 65&66, ACI 440 and ACI 544.

The methodology includes both temporary and permanent loads checks for the construction of tunnel lining segments. The methodology provides section resistance checks in ultimate state and in serviceability limit states. Additionally, mechanical checks as defined in fib Model Code (2012) are also provided. Finally, small-scale and full-scale tests have been performed.

Keywords: Fiber reinforced concrete, tunnel lining, glass fiber reinforced polymer bars

## ÖZ

### LİFLİ POLİMER DONATILI LİF KATKILI BETON TÜNELLERİN TASARIMI İÇİN BİR METOT

Demir, Mutlu  
Yüksek Lisans, İnşaat Mühendisliği  
Tez Danışmanı: Prof. Dr. Uğurhan Akyüz

Eylül 2019, 77 sayfa

Konvansiyonel donatılı prekast betonarme tünellerin inşaatında ve bakımında bazı zorluklar bulunmaktadır. Çelik donatıların paslanma sorunu yüzünden bu durum daha da karmaşık hale gelmektedir. Bunun yanı sıra, segmanların imalatı için gerekli olan işçilik çok zaman almaktadır. Lifli polimer donatı (FRP) içeren tünel segmanlarının tasarımı için bazı araştırmalar mevcuttur. Ayrıca, fiber katkılı beton (FRC) tünel kaplamalarının tasarımı ile ilgili de teknik kılavuzlar bulunabilmektedir.

Bu tez FRP donatı içeren fiber katkılı beton tünel kaplamalarının tasarımı ile ilgili bir metot önermektedir. Metot genel olarak fib Model Code 2010 (2012), bülten 65&66, ACI 440 ve ACI 544 şartnamelerinde yer alan öneri ve sınırlandırmalara dayanmaktadır.

Sunulan metot, tünel segmanlarındaki geçici ve kalıcı yük durumlarının kontrollerini içermektedir. Metot kesit taşıma dayanımı ile servis yükleri hesaplarını içermektedir. Ek olarak, lifli polimer donatılı fiber katkılı beton tünel kaplamalarının fib model code 2010 (2012)' da tanımlanan mekanik kriterlerin kontrolleri de bulunmaktadır. Son olarak küçük ölçekli ve tam ölçekli deneyler yapılmıştır.

Anahtar Kelimeler: fiber katkılı beton, tünel kaplamaları, cam elyaf takviyeli polimer donatı



To the memory of my uncle, H. Cüneyt Eskiyezli

## ACKNOWLEDGEMENTS

The author wishes to thank his supervisor Prof. Dr. Uğurhan Akyüz, for his valuable guidance throughout this study. His patience was limitless. Among many other things, being a decent man makes him inspirer.

The author would like to express his admiration to Prof. Dr. Uğur Ersoy, Prof. Dr. Ali Tuğrul Tankut and Prof. Dr. Güney Özcebe. They have done an extraordinary work at METU and I will always feel very privileged to study in their department. Whenever I run into trouble I opened their book and inspired by their work again and again.

The author would like to thank METU laboratory technicians, Barış Esen, Murat Demirel and Osman Keskin for their valuable help during the experimental study.

The author is thankful to his friends for their patience and support. My special thanks go to Emreca Polat.

The author wishes to thank to his mother, Şermin Demir, father, İzzettin H. Demir and sister Fulya Demir for their endless support and love.

Finally, the author is thankful to his wife, Ayşenur Kasımoğlu Demir for her patience. Without her encouragement, this thesis would not be completed.

## TABLE OF CONTENTS

ABSTRACT .....	v
ÖZ .....	vii
ACKNOWLEDGEMENTS .....	x
TABLE OF CONTENTS .....	xi
LIST OF TABLES .....	xiii
LIST OF FIGURES .....	xiv
LIST OF ABBREVIATIONS .....	xvii
CHAPTERS	
1. INTRODUCTION .....	1
1.1. General .....	1
1.2. Scope .....	1
1.3. Organization of the thesis .....	2
2. LITERATURE REVIEW .....	3
2.1. Introduction .....	3
2.2. Concrete Members reinforced with FRP bars .....	3
2.3. Fiber Reinforced Concrete Members .....	10
2.3.1. Characteristic Strength values for FRC .....	21
2.3.2. Shear Strength of FRC .....	22
2.4. Design of FRC Precast Concrete Tunnel Segments .....	24
2.4.1. Loading conditions .....	24
3. DESIGN OF FRC TUNNEL SEGMENTS WITH FRP REINFORCEMENT ..	39
3.1. Introduction .....	39

3.2. ULS Design.....	39
3.3. SLS Design .....	45
3.4. Mechanical Criteria.....	47
3.5. Design Checks for Precast FRC Tunnel Segments reinforced with FRP .....	49
3.6. Shear capacity of FRC segments reinforced with FRP .....	50
4. EXPERIMENTAL PROGRAM .....	51
4.1. Introduction.....	51
4.2. Test Specimens, Set-up and Material Properties .....	51
4.3. Full Scale Test Results .....	62
4.4. Small Scale Test Results .....	64
5. CONCLUSIONS .....	73
REFERENCES .....	75

## LIST OF TABLES

### TABLES

Table 2-1 Mechanical Properties of FRP Bars (fib Model Code 2010, 2012).....	4
Table 2-2 Mechanical Properties of FRP Bars (ACI 440.1R-15, 2015) .....	5
Table 2-3 Reduction factors in design codes for design of FRP reinforced sections (adopted from fib Model Code bulletin 40 2007) .....	10
Table 2-4 Partial Safety Factors for FRC.....	15
Table 2-5 $k_x$ values for different number of specimens (taken form RILEM, 2003).21	
Table 2-6 $k_n$ values for different number of samples (taken from ITAtech Report 7, 2016) .....	22
Table 2-7 Summary of design moment formulations for transient loading cases (adopted from ACI 544.7R-16, 2016).....	28
Table 2-8 Load factors for Service Loadings (ACI 544-7R-16, 2016).....	36
Table 4-1 Macro-Synthetic fiber properties .....	53
Table 4-2 Compressive strength values of test specimens taken from full-scale test member after bending test for İzmir Project .....	53
Table 4-3 GFRP mechanical Properties (taken from manufacturer test report) .....	54
Table 4-4 Beams test results according to EN 14651 .....	55
Table 4-5 Small-scale test specimen mixture and material properties.....	58
Table 4-6 Cracking Moment and Ultimate Moment values for full-scale bending tests .....	63
Table 4-7 Cracking moment and stresses for test specimens.....	67
Table 4-8 Ultimate Moment Capacities for Test-Specimen .....	68

## LIST OF FIGURES

### FIGURES

Figure 2-1 Assumed stress-strain diagram for FRP bars (fib Model Code 2010, 2012) .....	4
Figure 2-2 Strain- stress distributions in Ultimate Limit State for FRP reinforced concrete sections (ACI 440.1R-15, 2015) .....	8
Figure 2-3 Representation of Failure Modes for FRP reinforced concrete sections (CNR-DT 203, 2006).....	9
Figure 2-4 (a) softening, (b) hardening of FRC in tension (fib Model Code 2010, 2012) .....	10
Figure 2-5 Test Set-up according to EN 14651 .....	11
Figure 2-6 Schematic view of a beam for inverse analysis (fib Model Code 2010, 2012).....	12
Figure 2-7 Typical Load F-CMOD curve for plain concrete and FRC (fib Model Code 2010, 2012).....	13
Figure 2-8 Load F- CMOD curve for determination of $F_L$ .....	13
Figure 2-9 Simplified post-cracking constitutive laws (fib Model Code 2010, 2012) .....	14
Figure 2-10 Typical Strain & Stress relationship for FRC+RC sections (fib Model Code 2010 bulletin 66, 2012) .....	15
Figure 2-11 Stress-strain relations of FRC at SLS (a) softening (b,c) softening or hardening behavior (taken from fib Model Code 2010, 2012).....	16
Figure 2-12 Typical Load Displacement Curve for FRC .....	17
Figure 2-13 Stress-strain diagram and shape factor (Rilem TC 162, 2003).....	18
Figure 2-14 Stress-strain distribution (RILEM TC 162, 2003) .....	18
Figure 2-15 Strain-crack width relationship for FRC section (RILEM, 2003) .....	19

Figure 2-16 De-moulding loading case of tunnel segment (a) picture from manufacturing plant (b) idealized loads for de-moulding (ACI 544, 2016) .....	25
Figure 2-17 Storage of tunnel segments (a) picture from manufacturing plant (b) idealized loads for storage (ACI 544.7R-16, 2016) .....	26
Figure 2-18 Transportation of tunnel segments (a) picture from manufacturing plant (b) idealized loads for transportation (ACI 544.7R-16, 2016).....	27
Figure 2-19 Handling of tunnel segments (a) picture from manufacturing plant (b) idealized loads for handling (ACI 544.7R-16, 2016).....	28
Figure 2-20 Scheme of Thrust jacks of TBM (Meda et al, 2016).....	29
Figure 2-21 Spalling and bursting stress developed in segments due to TBM thrust (Liao et al., 2015) .....	29
Figure 2-22 Bursting stresses and parameters (a) by ACI 318 (b) German Tunneling Committee (2013) .....	30
Figure 2-23 Iyengar Diagram for calculation of bursting stresses (ACI 544.7R-16, 2016) .....	32
Figure 2-24 Schematic view of forces developed during tall-skin back grouting loading case (Groeneweg, 2007).....	33
Figure 2-25 Secondary grouting (Guglielmetti et al. 2007).....	34
Figure 2-26 Secondary grouting pressure over one-tenth of the lining (grouting pressure value is indicative) (Itatech report no: 22, 2019).....	34
Figure 2-27 Precast Segment load transfer with eccentricity and formation of split tensile stress (Daub, 2013) .....	37
Figure 3-1 Strain- stress distributions in ULS for FRP + FRC sections (for sections with $\epsilon_{uls} < \epsilon_{fu}$ ) .....	41
Figure 3-2 Strain- stress distributions at ULS for FRP+FRC sections (for sections with $\epsilon_{uls} \geq \epsilon_{fu}$ ) .....	42
Figure 3-3 Flowchart for calculation of Moment Capacity of FRC+FRP at ULS.....	43
Figure 3-4 N-M Diagram for FRC + GFRP section ( $f_{R3k} = 2.0$ MPa) and FRC section ( $f_{R3k} = 2.0$ MPa) .....	44

Figure 3-5 N-M Diagram for FRC + GFRP section ( $f_{R3k}=2.0$ MPa) and FRC section ( $f_{R3k}=4.0$ MPa) .....	45
Figure 3-6 Recommended reinforcement layout for precast tunnel linings (Tiberti et al. 2008) .....	46
Figure 4-1 Isometric View of TBM rings .....	52
Figure 4-2 Section view of TBM tunnels .....	52
Figure 4-3 Sectional reinforcement layout for precast segments .....	54
Figure 4-4 Load- CMOD curve for test beams in accordance with EN 14651 .....	56
Figure 4-5 Test setup for full scale bending test.....	58
Figure 4-6 Locations of LVDT's and strain gauges in full scale test (Tengilimoğlu, 2019).....	59
Figure 4-7 Additional LVDT's to measure compressive and tensional strain of the specimen .....	60
Figure 4-8 Small scale test set-up.....	61
Figure 4-9 Small scale test specimen support and loading locations .....	61
Figure 4-10 LVDT locations on small-scale test specimens .....	62
Figure 4-11 Load Deflection for full-scale bending tests .....	63
Figure 4-12 Moment Curvature Diagram for full-scale bending test, İzmir Project .	64
Figure 4-13 Load Deflection for small-scale bending tests.....	66
Figure 4-14 Load Deflection for small-scale bending tests, zoomed for cracking load .....	67
Figure 4-15 Location of cracks for Test beam -2 before failure.....	68
Figure 4-16 Location of cracks for Test beam -5 before failure.....	69
Figure 4-17 Moment-Curvature Diagram for small test specimen.....	70

## LIST OF ABBREVIATIONS

AFRP	Aramid Fiber Reinforced Polymer
CFRP	Carbon Fiber Reinforced Polymer
FRC	Fiber Reinforced Concrete
FRP	Fiber Reinforced Polymer
GFRP	Glass Fiber Reinforced Polymer
LOP	Limit of Proportionality
MSF	Macro-synthetic fiber
RC	Reinforced Concrete
RILEM	International Union of Laboratories and Experts in Construction Materials, System and Structures
SLS	Serviceability Limit State
SynFRC	Synthetic Fiber Reinforced Concrete
ULS	Ultimate Limit State



## CHAPTER 1

### INTRODUCTION

#### 1.1. General

The difficulties during construction and maintenance of tunnels force engineers to find alternatives to traditional construction techniques. Among these alternatives, the use of fibers in concrete (FRC) is rapidly increasing. Steel fiber composites and more recently synthetic fiber reinforced concrete (SynFRC) have been used in civil engineering structures. There are numerous tunnel projects composed of precast segments which was built by FRC.

The use of Fiber Reinforced Polymer (FRP) bars in civil engineering structures is also increasing nowadays due to its advantages compared to conventional reinforcement.

There are a number of design codes for the design of FRC elements. Moreover, design codes and guidelines for the design of FRC tunnel segments have been published recently. Design codes are also available for the design of structural concrete reinforced with FRP bars. However, there are not so many codes or guidelines for the design of FRC tunnel segments reinforced with FRP bars.

#### 1.2. Scope

In this study, a design procedure for FRC tunnel segments with FRP bars is presented. The study includes a design procedure for structural verification of bending moment – axial force interaction at ultimate limit states. Besides, the recommendations for serviceability limit state is also provided.

Moreover, mechanical criteria defined in fib Model Code 2010 (2012) for reinforced concrete members are modified for FRC segments with FRP bars.

Generally, shear is not the controlling parameter for the design of precast tunnel linings. However, it is recommended to check the shear capacity of tunnel segments as well (Itatech Report, 2016). Nonetheless, the shear capacity of FRC sections reinforced with FRP reinforcement is suggested to be checked by the equations provided in fib Model Code 2010 (2012).

### **1.3. Organization of the thesis**

This thesis consists of five chapters. Chapter 1 is the introduction part, presents the basic information for the subject, and defines the scope and organization of the thesis. Chapter 2, literature review, gives comprehensive information about the current design guidelines/codes. In the first part of Chapter 2, the design rules for concrete structures reinforced with FRP bars are discussed. In the second part, the design limitations/rules of FRC structures are provided. In the final part, the specific design rules of precast tunnel segments are presented. Loading conditions and design checks for tunnel linings are also provided.

In Chapter 3, a new design methodology is presented for FRC+FRP tunnel segments. First, the design rules at Ultimate Limit State (ULS) are presented. Second, the Serviceability Limit State (SLS) design is mentioned. Next, the mechanical criteria as defined in fib Model Code 2010 (2012) is reviewed. Finally, the equations for the calculation the shear capacity are proposed for FRC+FRP structures.

In Chapter 4, the test procedure and the test results for small-scale and full-scale tests are discussed.

In Chapter 5, the thesis is summarized and proposals for future studies are given.

## CHAPTER 2

### LITERATURE REVIEW

#### 2.1. Introduction

As there are limited codes or guidelines for FRP reinforced FRC tunnels, the studies are examined individually. In the first part, the contribution of FRP bars and the design limitations are discussed. In the second part, the discussions and design produces for FRC are reviewed.

#### 2.2. Concrete Members reinforced with FRP bars

In recent years, fiber reinforced polymer has become an alternative to conventional reinforcement in reinforced concrete members. There are a number of advantages of FRP when compared to conventional steel reinforcement. Some of the advantages are lower unit weight, high tensile strength, and non-corrosive properties. The transparency to magnetic fields and non-conductivity to electricity may also be considered as the advantages of Glass Fiber Reinforced Polymer (GFRP) bars (Caratelli et al., 2017). The disadvantageous of GFRP reinforcement can be listed as; lower modulus of elasticity and less bonding behavior compared to conventional steel reinforcement (Caratelli et al., 2016). Besides, FRP is vulnerable to creep and rupture under constant tension (ACI 440.1R-15, 2015).

There are a number of design guidelines and design codes for the use of FRP bars in concrete members as an alternative to steel reinforcement. According to ACI 440.1R-15 (2015), the design of concrete sections with FRP bars differs to the design methodology of conventional reinforced concrete sections. Since FRP bars have limited plastic behavior in tension, the behavior of the bars is assumed to be linear until failure. The same assumption is also accepted in fib Model Code 2010 (2012). The tensile behavior of FRP bar is presented in Figure 2-1. Moreover, the compression

capacity of the bars should not be taken into consideration in flexural calculations (ACI 440.1R-15).

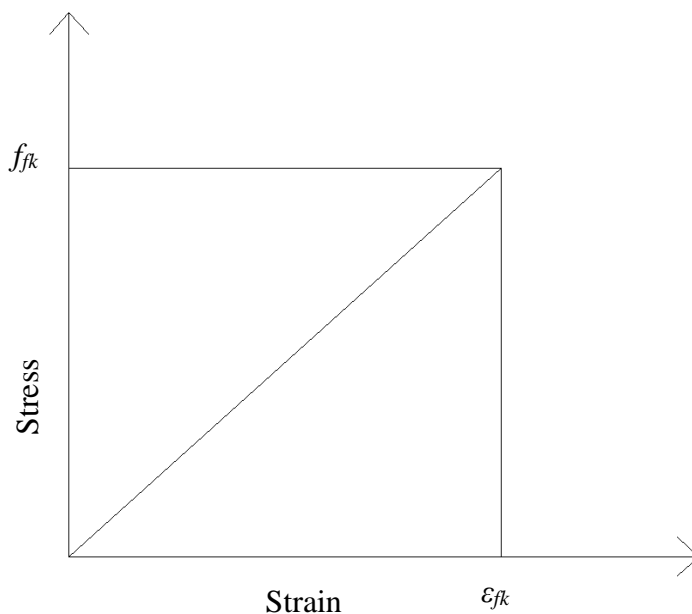


Figure 2-1 Assumed stress-strain diagram for FRP bars (fib Model Code 2010, 2012)

The mechanical properties of the FRP bars differs considerably compared to steel bars. There are several factors affecting the material properties. Some of them may be fiber type, orientation of fibers, dimensional effects, and quality control during manufacturing (ACI 440, 2015). The mechanical properties of FRP bars are determined by internationally accepted testing methods or procedures such as ACI 440.3R, ASTM D7205, ASTM D7337, ASTM D7705, Japan Society of Civil Engineers 1997b (ACI 440.1R-15 2015). The typical tensile properties of FRP bars are provided in Table 2-1 and Table 2-2.

Table 2-1 Mechanical Properties of FRP Bars (fib Model Code 2010, 2012)

	Carbon FRP	Glass FRP	Aramid FRP
Tensile Strength $f_{fu}$ (MPa)	600-3000	400-1600	600-2500
Modulus of elasticity $E_f$ (GPa)	80-500	30-60	30-125
Ultimate Strain $\epsilon_{fu}$ (%)	0.5-1.8	1.2-3.7	1.8-4.0

Table 2-2 Mechanical Properties of FRP Bars (ACI 440.1R-15, 2015)

	Carbon FRP	Glass FRP	Aramid FRP
Tensile Strength $f_{fu}$ (MPa)	600-3690	483-690	1720-2540
Modulus of elasticity $E_f$ (GPa)	120-580	35-51	41-125
Ultimate Strain $\varepsilon_{fu}$ (%)	0.5-1.7	1.2-3.1	1.9-4.4

Similar to conventional RC sections, the failure of concrete sections reinforced with FRP may be controlled by concrete crushing, balanced failure and by FRP rupture. Since FRP reinforcement does not yield, the balanced ratio for FRP reinforcement is lower than the conventional reinforcement (ACI 440.1R-15, 2015). Secondly, for FRP rupture failure mode, the equivalent rectangular stress block is not valid because the stress in extreme compression fiber is lower than the compressive strength. Typical failure modes in the ultimate state is shown in Figure 2-2. Reinforcement ratio and the balanced reinforcement of concrete sections reinforced with FRP bars can be calculated with Eq. (1) and Eq. (2):

$$\rho_f = \frac{A_f}{b d} \quad (1)$$

$$\rho_{fb} = 0.85 \beta_1 \frac{f'_c}{f_{fu}} \frac{E_f \varepsilon_{cu}}{E_f \varepsilon_{cu} + f_{fu}} \quad (2)$$

where;

$b$  = section width

$d$  = distance from compression side extreme fiber to center of reinforcement

$\rho_f$  = section reinforcement ratio

$\rho_{fb}$  = balanced reinforcement ratio

$\beta_1$  = factor for compressive stress calculation. Up to  $f'_c = 4000$  psi (28 MPa) it will be taken as 0.85. For higher values, the factor will be increased continuously by 0.05 per each 1000 psi (7 MPa). Minimum value is 0.65.

$f'_c$  = specified compressive strength of concrete

$E_f$  = design elastic modulus of FRP bars. It is equal to the mean modulus of test specimens ( $E_f = E_{f,ave}$ )

$\varepsilon_{cu}$  = ultimate concrete strain in compression

$\varepsilon_{fu}$  = design ultimate strain of FRP reinforcement

$$\varepsilon_{fu} = C_E \varepsilon_{fu}^*$$

$\varepsilon_{fu}^*$  = guaranteed rupture strain of FRP reinforcement. Can be calculated by average ultimate strain values of specimens minus three times standard deviation

$C_E$  = environmental reduction factor for FRP, given in Table 2-3

$f_{fu}$  = design ultimate strength of FRP reinforcement

$$f_{fu} = C_E f_{fu}^*$$

$f_{fu}^*$  = guaranteed rupture strength of FRP reinforcement. Can be calculated by average ultimate strength values of specimens minus three times standard deviation

The nominal flexural strength of FRP reinforced concrete sections for  $\rho_f > \rho_{fb}$  will be controlled by crushing of concrete limit state. Therefore, the moment capacity of the section can be calculated with Eq. (3).

$$M_n = \rho_f f_f \left( 1 - 0.59 \frac{\rho_f f_f}{f'_c} \right) b d^2 \quad (3)$$

If the section is controlled by FRP rupture limit state, then the reinforcement ratio is lower than the balanced ratio, i.e.,  $\rho_f < \rho_{fb}$ . The closed form equation has two unknowns, the concrete compressive strain and neutral axis depth. Moreover, the rectangular stress block approximation is not valid since the concrete in compression

zone does not reach to ultimate strain. Therefore, ACI 440.1R-15 (2015) proposes a conservative lower bound for ultimate moment capacity of section with Eq. (4) and Eq. (5) equations.

$$M_n = A_f f_{fu} \left( d - \frac{\beta_1 c_b}{2} \right) \quad (4)$$

$$c_b = \left( \frac{\varepsilon_{cu}}{\varepsilon_{cu} + \varepsilon_{fu}} \right) d \quad (5)$$

According to EN 1992-1-1 (2004), members without shear reinforcement the design shear resistance of conventional RC members can be calculated with Eq. (6).

$$V_{Rd,c} = [0.12 k (100 \rho_l f_{ck})^{\frac{1}{3}} + 0.15 \sigma_{cp}] b_w d \quad (6)$$

where;

$f_{ck}$  = characteristic compressive strength of concrete in MPa

$k = 1 + \left( \frac{200}{d} \right)^{0.5} \leq 2$  ;  $d$  is the section depth in mm

$\rho_l = A_{sl}/(b_w d) \leq 0.02$  ;  $A_{sl}$  is the area of tensile reinforcement

$b_w$  = smallest width of the cross-section in the tensile area (mm)

$\sigma_{cp} = \frac{N_{Ed}}{A_c} < 0.2 f_{cd}$  ;  $N_{Ed}$  is the axial force in section, for compression  $N_{Ed} > 0$  (N)

$A_c$  = concrete area (mm<sup>2</sup>)

fib Model Code Bulletin 40 (2007) modified Eq. (6) to Eq. (7) to account for the contribution of FRP bars.

$$V_{Rd,c} = [0.12 k (100 \rho_l \frac{E_f}{E_s} \phi_e f_{ck})^{\frac{1}{3}} + 0.15 \sigma_{cp}] b_w d \quad (7)$$

where;

$E_f$  = modulus of elasticity of FRP bars

$E_s$  = modulus of elasticity for steel bars

$\phi_e = \epsilon_f / \epsilon_y$  allowed strain of FRP bars divided by yield strain of steel

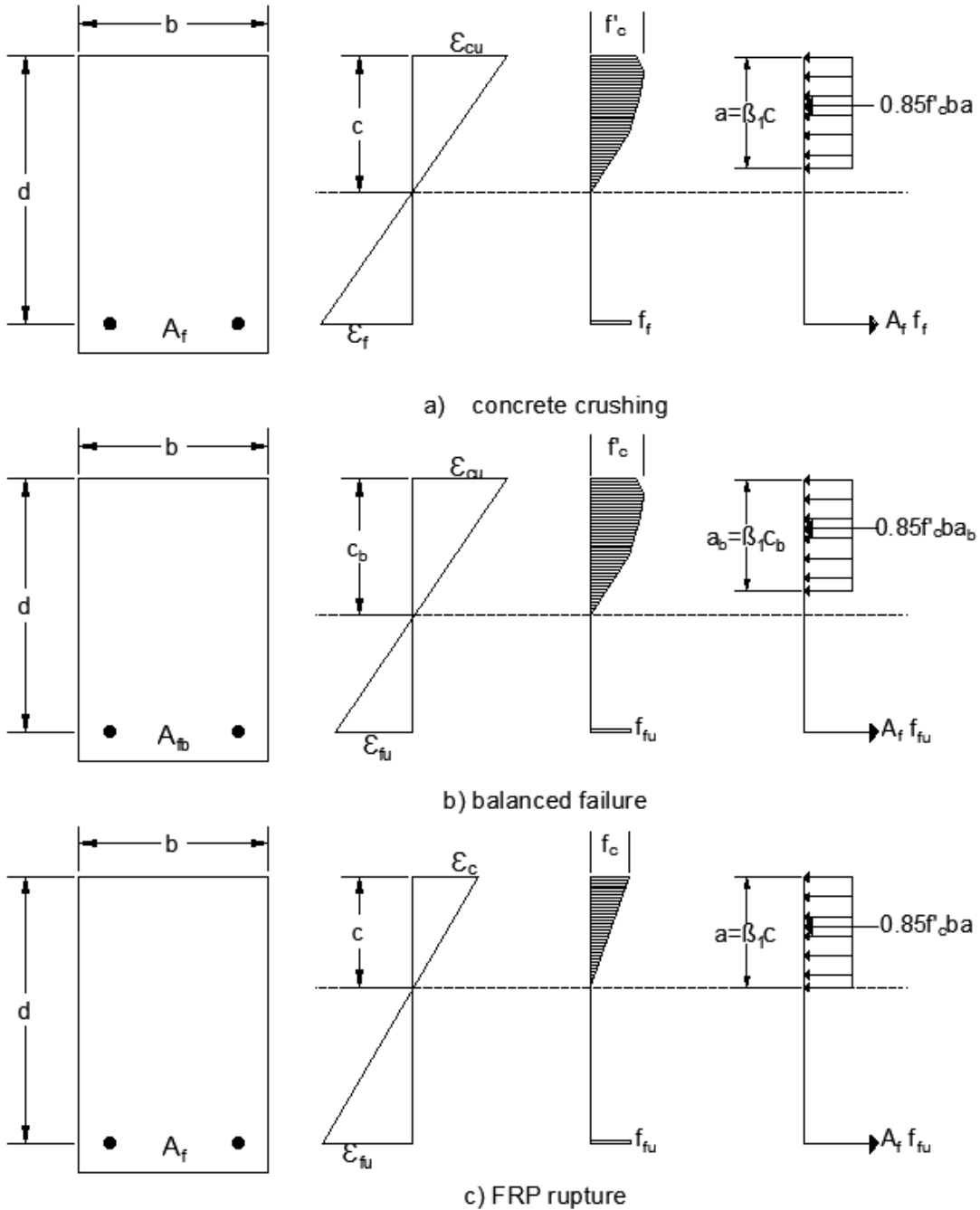


Figure 2-2 Strain- stress distributions in Ultimate Limit State for FRP reinforced concrete sections (ACI 440.1R-15, 2015)

For design at Serviceability Limit State (SLS), ACI 440.1R-15 (2015) limits the FRP bar stress for different material types. For example, the maximum tensile stress in FRP should be  $0.2f_{fu}$ ,  $0.3f_{fu}$  and  $0.55f_{fu}$  for GFRP, AFRP and CFRP, respectively (ACI 440.1R-15, 2015).

According to Italian National Research Council, CNR DT 203 (2006), the analysis at SLS includes stress limitation, deflection control and cracking control. The maximum stress in FRP bars exposed to moisture is limited to  $0.21f_{fu}$ ,  $0.40f_{fu}$  and  $0.81f_{fu}$  for glass, aramid and carbon, respectively. Further information may be found for deflection control and cracking control in CNR DT 203 (2006).

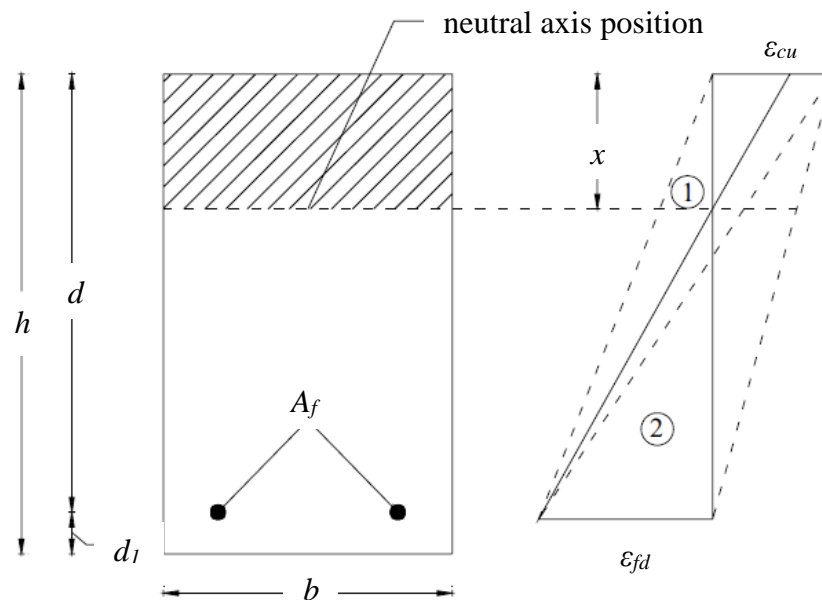


Figure 2-3 Representation of Failure Modes for FRP reinforced concrete sections (CNR-DT 203, 2006)

There are some design factors applied in design of FRP reinforced concrete sections. The tensile strength and strain of FRP bars are reduced with an environmental factor depending on the type of the FRP bars. Secondly, a conservative strength reduction factor is used in design calculations since FRP reinforced members exhibit a brittle behavior ACI 440.1R-15 (2015). The comparison between ACI 440.1R-15 (2015) and JSCE (Japanese Society of Civil Engineers) is shown in Table 2-3.

Table 2-3 Reduction factors in design codes for design of FRP reinforced sections (adopted from fib Model Code bulletin 40 2007)

Factor	ACI 440.1R-16	JSCE
Environmental Reduction factor	GFRP : 0.7-0.8 AFRP : 0.8-0.9 CFRP : 0.9-1.0	GFRP: 0.77 AFRP : 0.87 CFRP : 0.87
Strength Reduction Factor	$\Phi$ : 0.55-0.65 Total : GFRP : 0.39-0.52 AFRP : 0.44-0.59 CFRP : 0.50-0.65	GFRP: 0.77 AFRP : 0.87 CFRP : 0.87

### 2.3. Fiber Reinforced Concrete Members

Use of fibers in design of concrete members is increasing rapidly. Since the workmanship of conventional RC members is quite difficult, FRC members will become more popular.

The use of fibers may contribute to both Serviceability Limit State (SLS) and Ultimate Limit State ULS (fib Model Code 2010, 2012). The addition of fibers into concrete mixture would result in either hardening or softening behavior in concrete as shown in Figure 2-4. The contribution of fibers to concrete mixture does not show a great difference in uniaxial compression so majority of the design codes-guidelines does not take impact in compression into account (fib Mode Code 2010, 2012, ACI 544.7R-16, 2016).

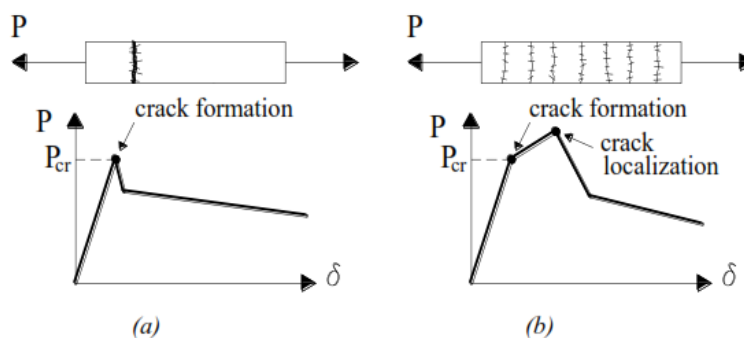


Figure 2-4 (a) softening, (b) hardening of FRC in tension (fib Model Code 2010, 2012)

For the design of FRC sections, a testing procedure is proposed in EN 14651. The test set-up is illustrated in Figure 2-5. The test procedure is for metallic fibers or a combination of metallic fibers and other type of fibers. However, it may also be applied for other types of fibers. The aim of the testing procedure is to determine the load- Crack Mouth Opening Displacement (CMOD) curve.

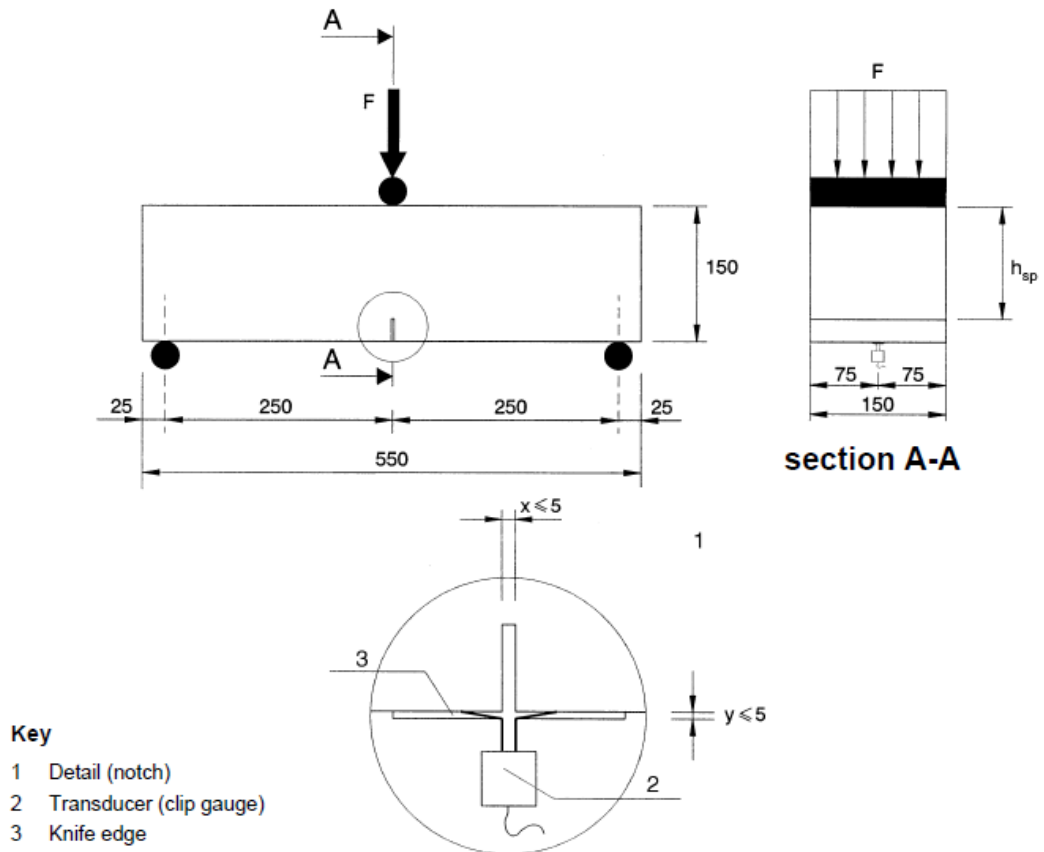


Figure 2-5 Test Set-up according to EN 14651

After getting the load-CMOD curve, one can get stress-crack opening with inverse analysis as mentioned in fib Model Code 2010 (2012) or ACI 544.7R-16, (2016). In inverse analysis, the section is divided into a number of fictitious crack openings. Then equilibrium calculation is performed for every opening as shown in Figure 2-6. ACI 544.7R-16, (2016) provides a spreadsheet for the calculation of design parameters. For a simpler approach, the design parameters may also be calculated with approximations as stated in EN 14651.

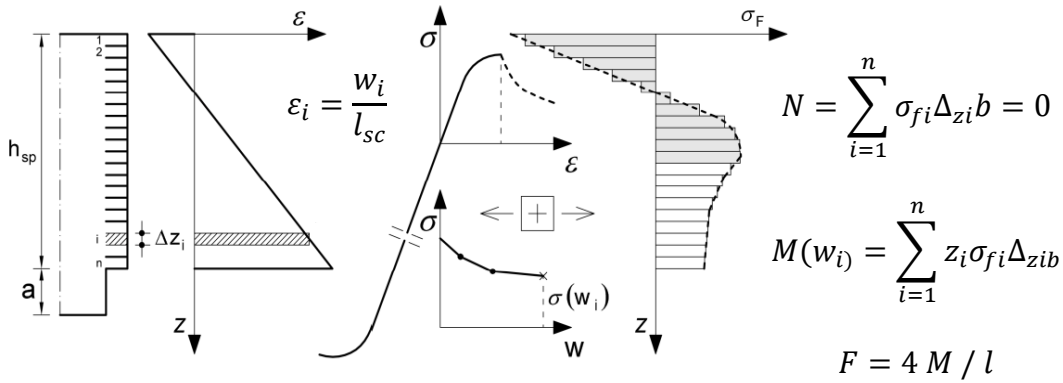


Figure 2-6 Schematic view of a beam for inverse analysis (fib Model Code 2010, 2012)

After plotting Load-CMOD curve stress values can be calculated with Eq. (8). A typical load-deformation curve for FRC and plain concrete is presented in Figure 2-7.

$$f_{R,j} = \frac{3 F_j l}{2 b h_{sp}^2} \quad (8)$$

where;

$f_{R,j}$  = residual flexural tensile strength corresponding to CMOD = CMOD<sub>j</sub>

$F_j$  = load corresponding to CMOD = CMOD<sub>j</sub>

$l$  = span length

$b$  = width of the specimen

In order to calculate Limit of Proportionality (LOP), a line is drawn at a distance of 0.05mm parallel to the load axis of Load- CMOD curve. The highest load between 0 to 0.05mm is accepted as the  $F_L$  value as shown in Figure 2-7.

Based on the bending test results two approximations can be made: a plastic rigid behavior or linear-post cracking behavior as shown in Figure 2-9 (fib Model Code 2010, 2012). If the rigid plastic model is assumed, then ultimate residual strength can be approximated with Eq. (9).

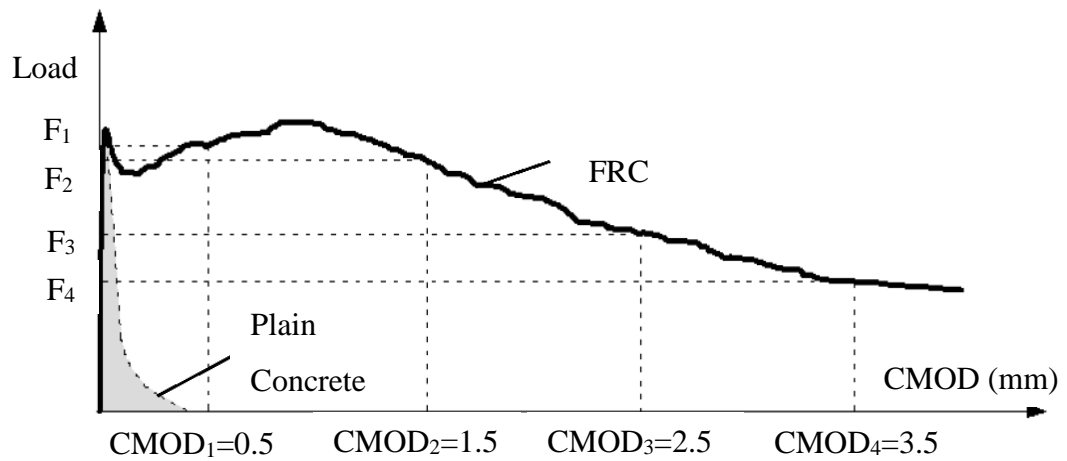


Figure 2-7 Typical Load F-CMOD curve for plain concrete and FRC (fib Model Code 2010, 2012)

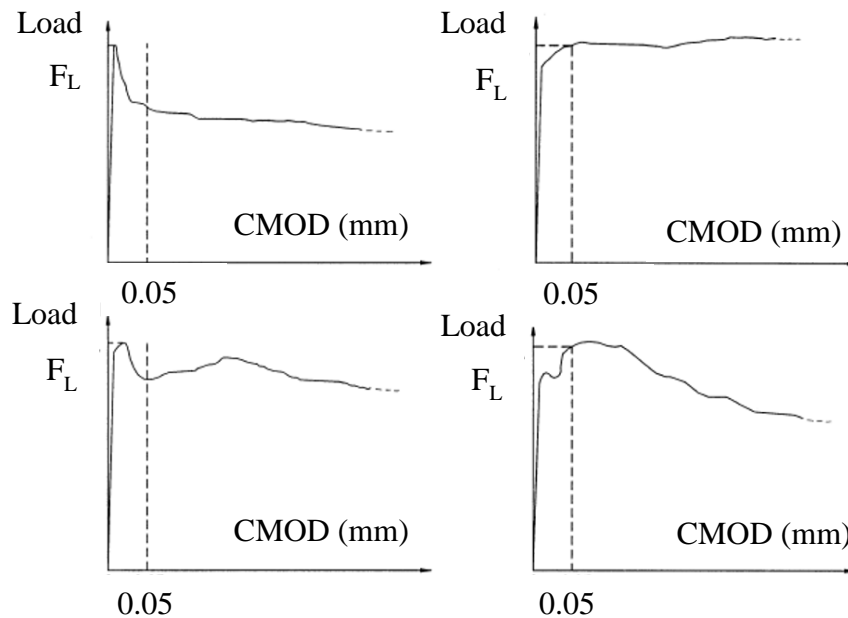


Figure 2-8 Load F- CMOD curve for determination of  $F_L$

$$f_{Ftu} = f_{R3} / 3 \quad (9)$$

where;

$f_{Ftu}$  = ultimate residual strength

$f_{R3}$  = strength value at 2.5mm crack opening. i.e., at  $CMOD_3$

If linear post-cracking model is assumed, Eq. (10) and Eq. (11) can be used:

$$f_{Fts} = 0.45 f_{R1} \quad (10)$$

$$f_{Ftu} = f_{Fts} - \frac{w_u}{CMOD_3} (f_{Fts} - 0.5 f_{R3} + 0.2 f_{R1}) \geq 0 \quad (11)$$

where;

$w_u$  = maximum permitted crack opening.

For precast tunnel segments, fib model code 2010 (2012) proposes to calculate the strain as:

$$\varepsilon = w/l_{sc} \quad (12)$$

where;

$l_{sc}$  = structural characteristic length and may be taken as  $d$  (depth of section)

$w$  = crack width

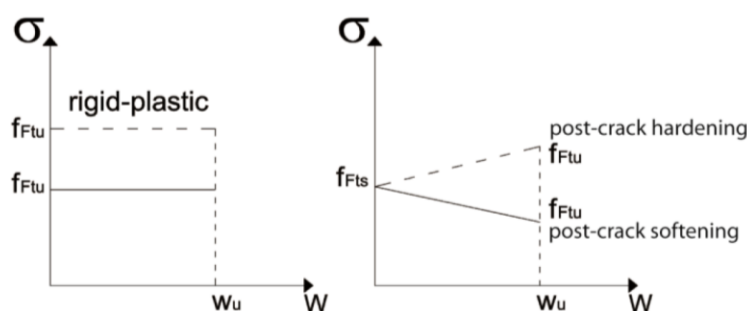


Figure 2-9 Simplified post-cracking constitutive laws (fib Model Code 2010, 2012)

The sectional resistance at ULS may be calculated in accordance with the strain and stress relationship as shown in Figure 2-10.

The stress-strain relations at SLS is also provided in fib Model code 2010 (2012). According to the behavior of the material, i.e., softening or hardening, the stress-strain relation may differ. This is presented in Figure 2-11. The limiting strain values are defined as;

$$\varepsilon_{sls} = CMOD_1/l_{cs} \quad (13)$$

$$\varepsilon_{uls} = \min(\varepsilon_{fu}, \frac{2.5}{l_{cs}}) \quad (14)$$

$\varepsilon_{fu}$  = maximum permitted tensile strain and it can be taken as 2.0% for variable strain distribution (fib Model Code 2010, 2012).

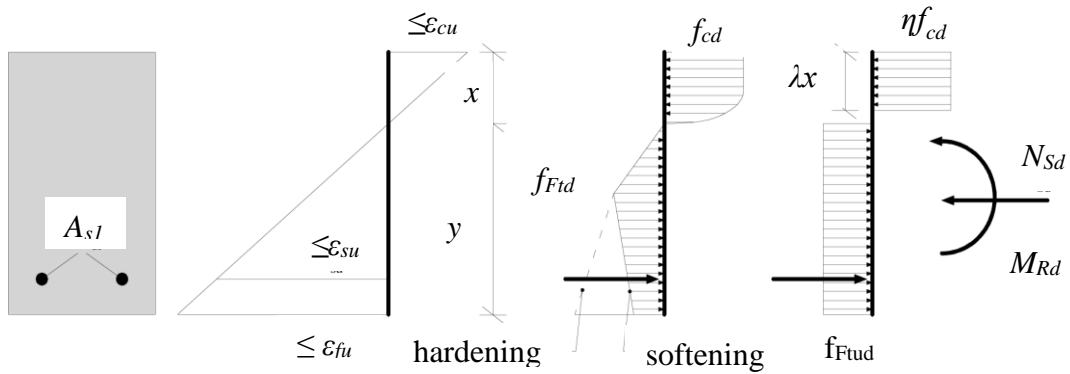


Figure 2-10 Typical Strain & Stress relationship for FRC+RC sections (fib Model Code 2010 bulletin 66, 2012)

The material factors recommended in fib Model Code 2010 (2012) is provided in Table 2-4.

Table 2-4 Partial Safety Factors for FRC

Material	Partial Safety Factor
FRC in compression	As plain concrete
FRC in tension	$\gamma_F = 1.5$

According to fib Model code 2010 (2012), it is permitted to replace conventional reinforcement with fiber reinforcement if the following relations are satisfied:

$$f_{R1k}/f_{RLk} > 0.4 \quad (15)$$

$$f_{R3k}/f_{R1k} > 0.5 \quad (16)$$

where;

$f_{RLk}$  = characteristic value of Limit of Proportionality

$f_{R1k}$  = characteristic strength value at 0.5mm crack opening. i.e., at  $CMOD_1$

$f_{R3k}$  = characteristic strength value at 2.5mm crack opening. i.e., at  $CMOD_3$

Additionally one of the following conditions shall also be satisfied:

$$\delta_u \geq 20\delta_{SLS} \quad (17)$$

$$\delta_{peak} \geq 5\delta_{SLS} \quad (18)$$

$\delta_u$  is the ultimate displacement,  $\delta_{peak}$  is displacement where maximum load occur,  $\delta_{SLS}$  is the displacement at SLS, calculated with uncracked concrete and initial elastic modulus assumptions. These variables are illustrated in Figure 2-12. Finally, the ultimate load ( $P_u$ ) should be higher than cracking load ( $P_{cr}$ ) and service load ( $P_{SLS}$ ).

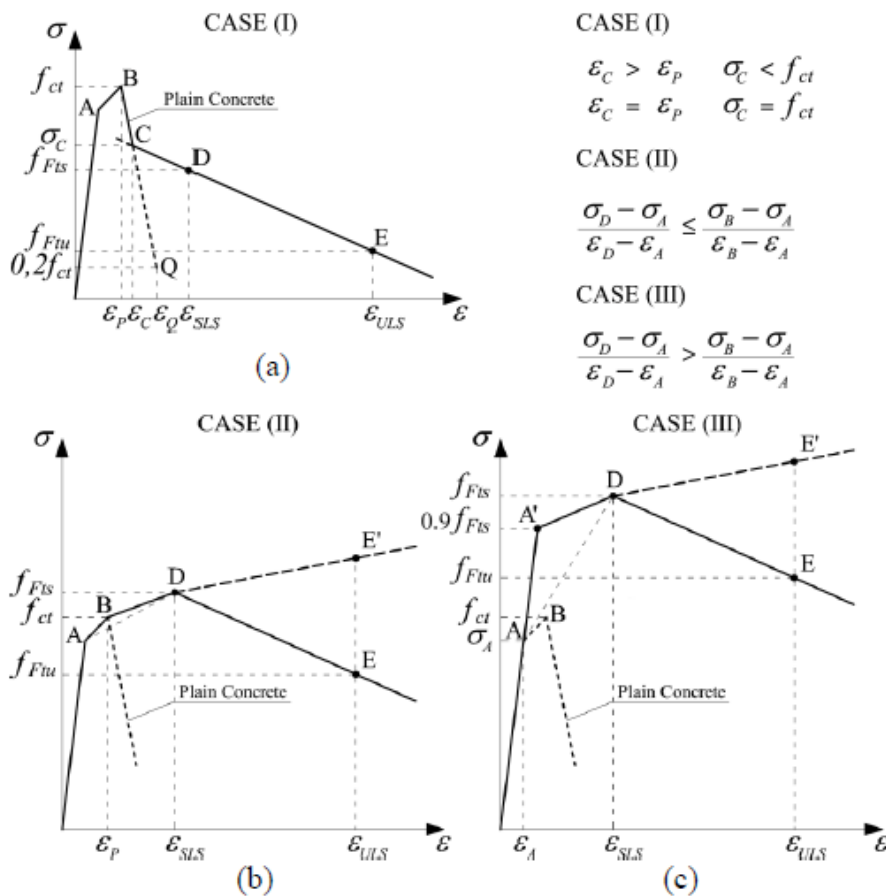


Figure 2-11 Stress-strain relations of FRC at SLS (a) softening (b,c) softening or hardening behavior (taken from fib Model Code 2010, 2012)

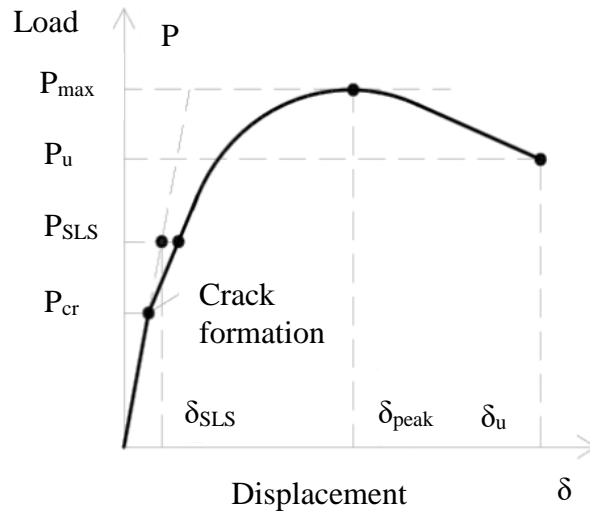


Figure 2-12 Typical Load Displacement Curve for FRC

A similar design methodology is proposed in ACI 544.7R-15 (2015). The design parameters are determined by ASTM C1609/C1609M beam test instead of EN 14651. Besides, the limiting values for strain and stress and material factors differs. A similar approach is also proposed in RILEM TC-162 (2003). The stress strain diagram for FRC is shown in Figure 2-13.

According Rilem TC 162 (2003), the proposed method shows a major difference from the experimental results for different sizes. So a size factor is introduced in the design calculations. RILEM also recommends further research for the reason of this size effect. The stress-strain distribution is given in Figure 2-14.

RILEM limits the maximum crack width by 3.5mm which is 2.5mm in fib Model Code 2010 (2012). The crack width calculation in RILEM is also different from the Model Code. For sections without reinforcement bars, the tension strain can be calculated with the following equation:

$$\varepsilon_{fc,t} = \varepsilon_{fc,max} \frac{h - x}{x} \quad (19)$$

The crack width for FRC sections at ULS can be:

$$w = \varepsilon_{f_c,t} (h - x) \quad (20)$$

The schematic view of the crack width in FRC sections is represented in Figure 2-15.

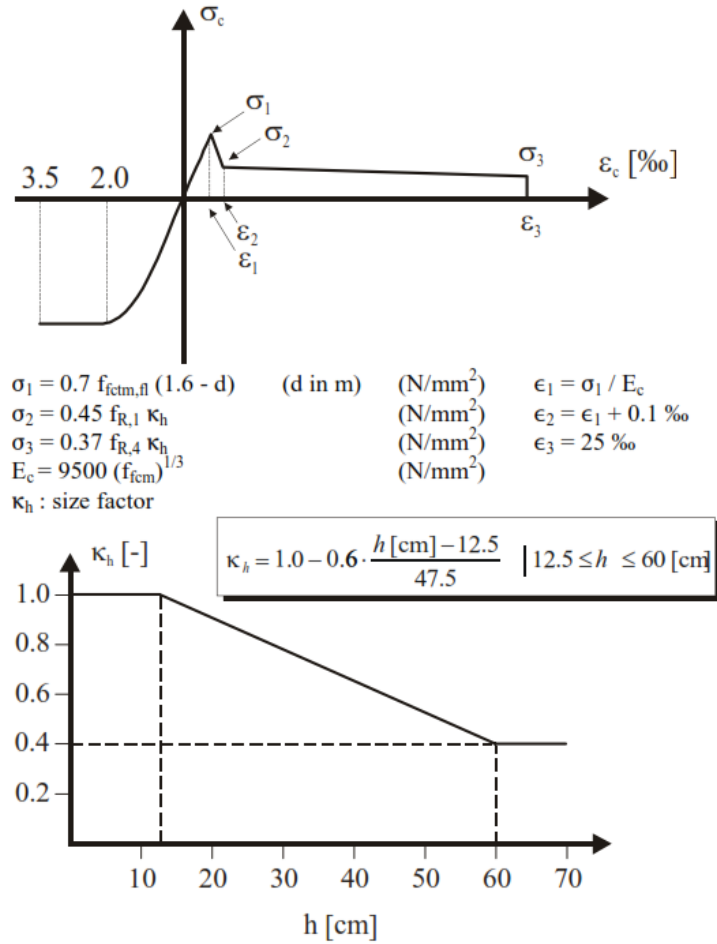


Figure 2-13 Stress-strain diagram and shape factor (Rilem TC 162, 2003)

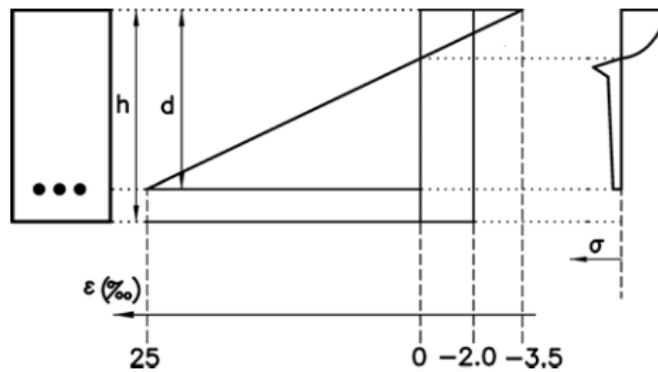


Figure 2-14 Stress-strain distribution (RILEM TC 162, 2003)

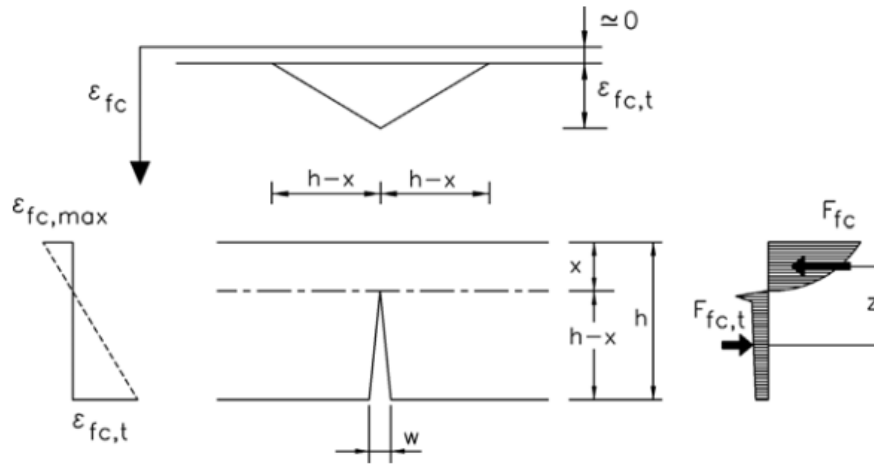


Figure 2-15 Strain-crack width relationship for FRC section (RILEM, 2003)

For the design at SLS, the fib Model Code 2010 (2012) limits both compressive and tensile stresses in the section. fib Model Code 2010 (2012) limits the maximum compressive stress to  $0.6f_{ck}$ . According to EN 1992-1-1 (2004), for conventional RC sections the maximum compressive stresses is limited to  $0.6f_{ck}$  and  $0.45f_{ck}$  for characteristic combination and quasi-permanent loads combination respectively. The values are recommended values and the designer may change these values according to national annex.

Secondly, the tensile stress in FRC elements is limited to  $0.6F_{f_{tsk}}$  (fib Model Code 2010, 2012).  $F_{f_{ts}}$  can be calculated with Eq. (10). The crack opening value limit should be satisfied. The limit is generally between 0 and 0.3mm (Di Carlo et al. 2016).

To prevent any unpredicted sudden failures, the minimum reinforcement area concept is widely used in conventional reinforced concrete sections where tension is expected. The equation given in EN 1992-1-1 (2004) for minimum reinforcement area may also be used for FRC sections with some modification. The moment capacity after cracking of the section due to fibers should be introduced in the equation. So, as stated by RILEM, the equation becomes:

$$A_{s,min} \sigma_s = (k_c k k_p f_{fct,eff} - 0.45 f_{Rm,1}) A_{ct} \quad (21)$$

where;

$A_{s,min}$  = minimum reinforcement area

$\sigma_s$  = permitted reinforcement stress. It may be taken as yield stress however; a lower value may be required for the crack width limitations

$l_{sc}$  = structural characteristic length and can be taken as  $d$  (depth of section)

$k_c$  = coefficient to account for the stress distribution.  $k_c = 1$  for pure tension;  $k_c = 0.4$  for pure bending

$k_p$  = coefficient for prestressed member;  $k_p$  is taken as 1 for non-prestressed members

$f_{Rm,1}$  = average residual flexural tensile strength of FRC at 0.5mm crack opening (CMOD<sub>1</sub>)

$f_{ct,eff}$  = cracking tensile strength of concrete,  $f_{ctm}$

$A_{ct}$  = the are in the tensile zone

Obviously, if the right side of the equation is negative there is no need for additional reinforcement (Rilem TC 162, 2003).

A similar formulation for minimum reinforcement is also provided in bulletin 66 of fib Model Code 2010 (2012).

$$A_{s,min} \sigma_s = (k_c k f_{ctm} - f_{Ftsm}) A_{ct} \quad (22)$$

where;

$f_{Ftsm}$  = average residual strength of FRC

$\sigma_s$  = steel stress but, it is recommend to be taken as yield stress

$k_c$  = coefficient that was previously defined but for rectangular sections it is recommended to be taken as  $k_c = 1$

### 2.3.1. Characteristic Strength values for FRC

According to RILEM, the characteristic strength values for FRC sections, where bending tests are available, can be calculated with the following equation;

$$f_{ctk,l} = f_{ctm,l} - k_x s_p \quad (23)$$

where;

$f_{ctk,l}$  = characteristic value of the limit of proportionally (LOP) from the procedure defined previously in Figure 2-8 and Eq. (8)

$f_{ctm,l}$  = mean value of LOP

$$s_p = \sqrt{\frac{\sum(f_{fctm,L} - f_{fct,L})^2}{(n - 1)}}$$

$n$  = number of specimens

$k_x$  = coefficient to consider the number of specimens, can be taken from Table 2-5. If the coefficient of variation of the population is known then the values in  $k_{xknown}$  should be used, otherwise, the values in  $k_{xunknown}$  row will be taken.

Table 2-5  $k_x$  values for different number of specimens (taken form RILEM, 2003)

n	1	2	3	4	5	6	8	10	20	30	$\infty$
$k_{xknown}$	2.31	2.01	1.89	1.83	1.80	1.77	1.74	1.72	1.68	1.67	1.64
$k_{xunknown}$	-	-	3.37	2.63	2.33	2.18	2.00	1.92	1.76	1.73	1.64

According to Itatech Report n.7 (2016), the characteristic flexural tensile strength of FRC can be determined with the following equation:

$$f_{ctk} = f_{fctm} (1 - k_n V_x) \quad (24)$$

$f_{ctk}$  = characteristic flexural strength of FRC

$f_{fctm}$  = mean FRC flexural tensile strength

$V_x$  = coefficient of variation, standard deviation of  $f_{ct}$  divided by mean  $f_{ctm}$

$k_n$  = a coefficient based on number of samples

Eq. (24) can also be used for residual strength parameters (Itatech Report n.7, 2016). The values of  $k_x$  and  $k_n$  shows similarity in Table 2-5 and Table 2-6. Itatech Report n.7 (2016) states that, the  $k_n$  values for the known  $V_x$  should be used in design calculations since there are a number of beam test results for FRC. Another important information stated in the Itatech report n.7 (2016) is the use of  $k_n$  values for %5 and 95% probabilities. According to Itatech, for SLS and ULS verification calculations the characteristic strength should be calculated with %5 lower fractile estimation. However, for crack width calculations, it is permitted to use %95 reliable estimate of the mean value.

Table 2-6  $k_n$  values for different number of samples (taken from ITatech Report 7, 2016)

Number of Samples	$k_n$ , Mean for 95% ( $k_n = 1.64 N^{-0.5}$ ) ( $V_x$ : known)	$k_n$ , Mean for 5% ( $k_n = 1.64 N^{-0.5}$ ) $V_x$ : known)	$k_n$ , Mean for 5% $V_x$ : unknown)
3	0.95	1.89	3.37
6	0.67	1.77	2.16
12	0.47	1.71	1.89
>30	0.00	1.64	1.64

### 2.3.2. Shear Strength of FRC

Although shear forces is not governing in design of FRC tunnel segments mostly, it is required to check the shear capacity of the section (Itatech report no:16, 2016). fib Model Code 2010 (2012) recommends formulas for the shear capacity of FRC sections. If the section is without reinforcement then Eq. (25) should apply.

$$\sigma_1 \leq f_{Ftuk} / \gamma_f \quad (25)$$

where;

$\sigma_1$  = principal tensile strength

$f_{Ftuk}$  = characteristic ultimate tensile strength of FRC determined according to Eq. (11) for  $w_u = 1.5\text{mm}$

$\gamma_f$  = material factor as defined in Table 2-4

If the section includes longitudinal reinforcement only, the shear capacity can be calculated with formula given in fib Model Code 2010 (2012). For FRC sections satisfying Eq. (26) the minimum shear reinforcement is not required.

$$0.08 (f_{ck})^{0.5} \leq f_{Ftuk} \quad (26)$$

$f_{Ftuk}$  = characteristic ultimate tensile strength of FRC determined according to Eq. (11) for  $w_u = 1.5 \text{ mm}$

According to fib Model Code 2010 (2012), Eq. (27) can be used for the calculation of the shear resistance for members with conventional longitudinal reinforcement and without shear reinforcement. In fact, the equation is similar to Eq. (6) with the modification of additional contribution of FRC.

$$V_{Rd,c} = \left\{ 0.12 k \left[ 100 \rho_l \left( 1 + 7.5 \frac{f_{Ftuk}}{f_{ctk}} \right) f_{ck} \right]^{1/3} + 0.15 \sigma_{cp} \right\} b_w d \quad (27)$$

where;

$k = 1 + \left( \frac{200}{d} \right)^{0.5} \leq 2$  ; d is the section depth in mm

$\rho_l = A_{sl}/(b_w d) \leq 0.02$  ;  $A_{sl}$  is the area of tensile reinforcement

$f_{ck}$  = characteristic compressive strength of concrete in MPa

$f_{Ftuk}$  = characteristic ultimate tensile strength of FRC determined according to Eq.(11) for  $w_u = 1.5 \text{ mm}$

$f_{ctk}$  = characteristic value of tensile strength of concrete without fibers in MPa

$f_{ck}$  = characteristic compressive strength of concrete in MPa

$$\sigma_{cp} = \frac{N_{Ed}}{A_c} < 0.2f_{cd} ; N_{Ed} \text{ is the axial force in the cross-section, for compression}$$

$$N_{Ed} > 0 (N)$$

$b_w$  = smallest width of the cross-section in the tensile area (mm)

$A_c$  = concrete area (mm<sup>2</sup>)

## **2.4. Design of FRC Precast Concrete Tunnel Segments**

There are some design codes/guidelines for the design of fiber-reinforced precast tunnel segments. Most of these codes are for steel fiber reinforced members. Limitations for the design of FRC precast tunnel segments can be applied for other types of fibers such as synthetic fibers by applying additional small scale and full-scale tests (ACI 544.7R-16, 2016).

### **2.4.1. Loading conditions**

The loading conditions of FRC precast concrete tunnel segments may be divided into three main stages: transient stage loads, loads for construction stage and loads for service stages.

The transient stage includes the de-moulding, storage, transportation and handling of the precast tunnel segments. In all of the transient stages the section is subjected to bending moment without axial forces.

Segment de-moulding process and the idealized loading is shown in Figure 2-16. The design calculations shall include the design strength of concrete at the time that the process will be implemented. It should be noted that in many of the projects, the compressive strength of concrete is expected to be 15 MPa after 3.5-4 hours of concrete pouring (ACI 544.7R-16, 2016). The early-age concrete strength, both in tension and compression, is important. The bending moment is resulting from the self-weight of the segment. A load factor should be used in accordance with the national standards. According to ACI 544.7R-16 (2016), a load factor of 1.4 should be adopted for design.

It is also important that, the concrete strength at this stage has not reached to ultimate strength since the process will start less than 28-days. Therefore, the calculations shall be done accordingly. According to Itatech Report no:16 (2016), the de-moulding phases should be analyzed in both SLS and ULS. The segments shall be evaluated with standard test specimens having the same curing time and curing procedure.

In addition to the capacity checks for flexural strength, the shear capacity shall also be calculated (Itatech Report no: 16, 2016).

According to Itatech Report no: 16 (2016), the SLS check for this loading condition can be performed with the assumption that the concrete is in uncracked state. Therefore, the maximum tensile stress should be less than the tensile strength of concrete during de-moulding. In other words, the following equation should be satisfied:

$$\sigma_{1,2} \leq f_{ctk,0.05(t)} \quad (28)$$

where;

$\sigma_{1,2}$  = maximum principle tensile stress calculated from the combination of axial loads, shear forces and bending moments.

$f_{ctk,0.05(t)}$  = tensile strength of concrete at the time, t. Here t is equal to de-moulding time.

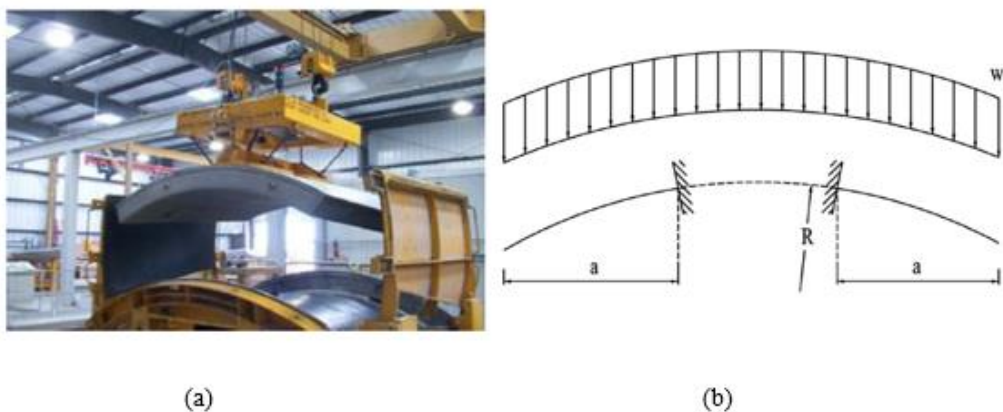
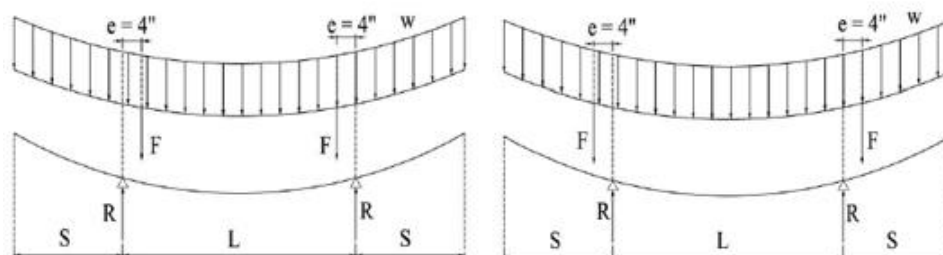


Figure 2-16 De-moulding loading case of tunnel segment (a) picture from manufacturing plant (b) idealized loads for de-moulding (ACI 544, 2016)

After de-moulding of segments, they will be stored in the storage yard. The segments are stored on top of each other with wood support between them and at the ground floor as it is in Figure 2-17.



(a)



(b)

(c)

Figure 2-17 Storage of tunnel segments (a) picture from manufacturing plant (b) idealized loads for storage (ACI 544.7R-16, 2016)

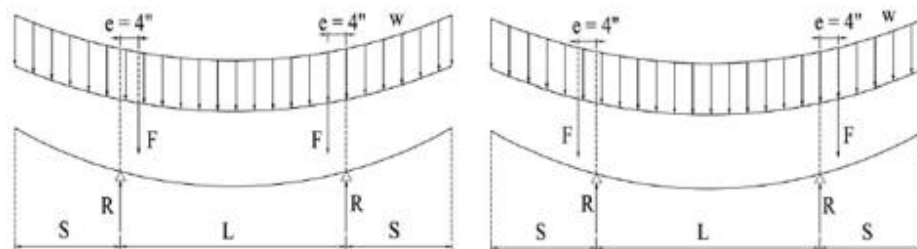
In theory, if the wood supports are placed in straight line, the segment will not be subjected to any bending moment. However, in practice this may not be the case. Therefore, for design purposes 100mm eccentricity is accepted between the wood supports (ACI 544.7R-16, 2016). This eccentricity may be inside or outside of the wood blocks. Both of these loading cases may be modeled as simply supported beam as shown in Figure 2-17 (b) & (c). As it is in the de-moulding stage, this stage does not include any load other than the self-weight of the segments. So the same load factor, 1.4, can be used in design (ACI 544.7R-16, 2016).

Capacity checks for storage stage is similar to the ones in de-moulding. The cracks should be avoided as much as possible. Eq. (28) is also valid for this loading case. Both SLS and ULS design checks should be done (Itatech Report no:16, 2016).

The storage of the segments are shown in Figure 2-18. Capacity checks for storage stage is similar to the ones in de-moulding and storage. The cracks should be avoided as much as possible. Eq. (28) is also valid for this loading case. Both SLS and ULS calculations should be done (Itatech Report no:16, 2016).



(a)



(b)

(c)

Figure 2-18 Transportation of tunnel segments (a) picture from manufacturing plant (b) idealized loads for transportation (ACI 544.7R-16, 2016)

Segment handling from storage area is usually done with special devices such as vacuum lifters (ACI 544.7R-16, 2016). The typical example of segment handling and the corresponding loading scheme is shown in Figure 2-19. The loading case is very

similar to de-moulding load case. Therefore, the design forces can be calculated with same formulations.

The capacity checks for handling is similar to the ones in previous loading cases. Eq. (28) can be used for this loading case. Both SLS and ULS calculations should be performed (Itatech Report no:16, 2016).

The calculation of unfactored design moments is given in Table 2-7.

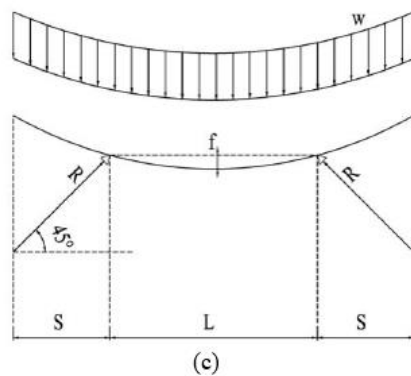
Table 2-7 Summary of design moment formulations for transient loading cases (adopted from ACI 544.7R-16, 2016)

Load Case	Dynamic shock factor	Maximum moment (unfactored)
De-moulding	-	$wa^2/2$
Storage	-	$w(L^2/8-S^2/2)+F_1e$ or $w(S^2/2)+F_1e$
Transportation	2.0	$w(L^2/8-S^2/2)+F_2e$ or $w(S^2/2)+F_2e$
Handling	2.0	$wa^2/2$



(a)

(b)



(c)

Figure 2-19 Handling of tunnel segments (a) picture from manufacturing plant (b) idealized loads for handling (ACI 544.7R-16, 2016)

The segments are subjected to significant bursting, spalling and compressive stresses during the advance of TBM. Due to the thrust of TBM, compressive stress occur under the jacks. The high compressive forces results in spalling and bursting tensile stresses in the segment as shown in Figure 2-21.

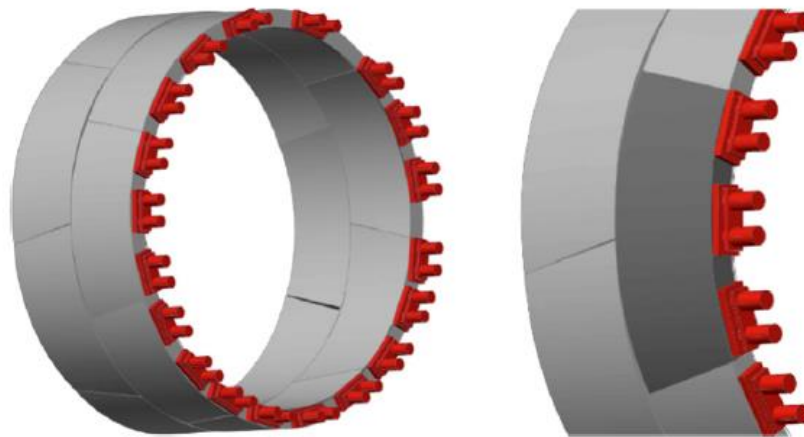


Figure 2-20 Scheme of Thrust jacks of TBM (Meda et al, 2016)

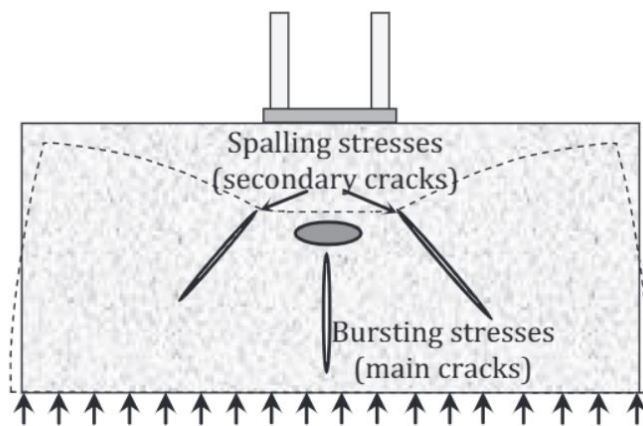


Figure 2-21 Spalling and bursting stress developed in segments due to TBM thrust (Liao et al., 2015)

The analysis for the sectional response may be performed by simplified equations, analytical methods, finite-element analysis (2D/3D) or by nonlinear fracture mechanic analyses. According to ACI 544.7R-16 (2016) the bursting force,  $T_{burst}$  and the location of the force,  $d_{burst}$  may be calculated by the simplified equations recommended by ACI 318. ACI 544.7R-16 (2016) also states that the equations in

German Tunneling Committee (2013) may also be used for the calculations of bursting force.

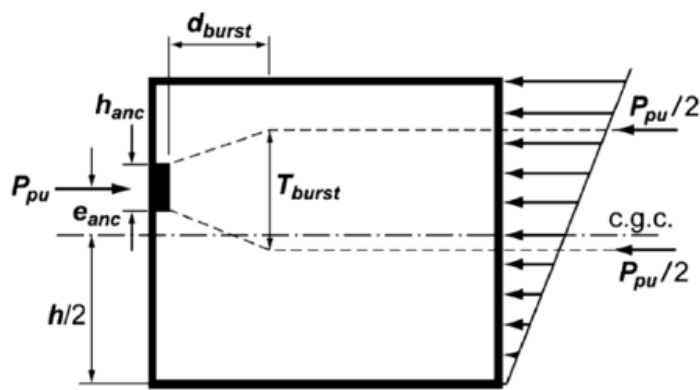
According to ACI 318:

$$T_{burst} = 0.25 P_{pu} (1 - h_{anc}/h); d_{burst} = 0.5 (h - 2e_{anc}) \quad (29)$$

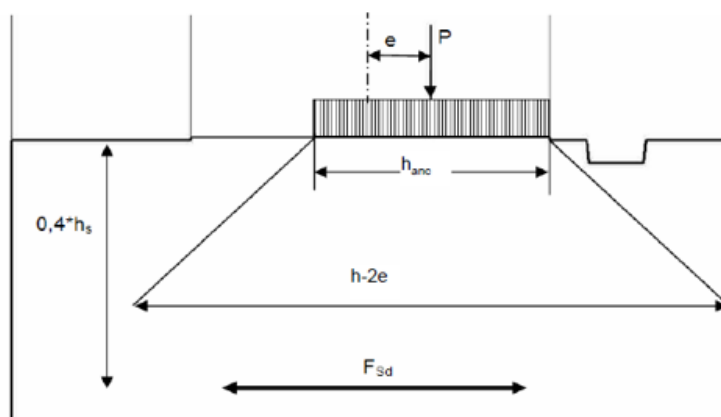
According to German Tunneling Committee:

$$T_{burst} = 0.25 P_{pu} (1 - h_{anc}/(h - 2e_{anc}); d_{burst} = 0.5 (h - 2e_{anc}) \quad (30)$$

The parameters for the equations are shown in Figure 2-22.



(a)



(b)

Figure 2-22 Bursting stresses and parameters (a) by ACI 318 (b) German Tunneling Committee (2013)

The eccentricity,  $e_{anc}$  is specified by the TBM manufacturer. If the  $e_{anc}$  is not provided, it can be taken as 30mm (ACI 544.7R-16, 2016). The radial and transverse bursting stresses can be determined with following equations:

$$\sigma_{p,r} = T_{burst} / \Phi a_l d_{burst} \quad (\text{radial direction}) \quad (31)$$

$$\sigma_{p,t} = T_{burst} / \Phi h_{anc} d_{burst} \quad (\text{tangential direction}) \quad (32)$$

where;

$\Phi$  = strength reduction factor and equal to 0.7 according to ACI 544.7R-16 (2016)

$a_l$  = transverse length of jack shoe

The bursting stresses must be checked with the residual tensile strength of FRC tunnel segments. If the bursting stresses are higher than the residual strength, additional reinforcement bars may be used. In such a case, according to ACI 544.7R-16 (2016) the following formulations can be used:

$$T_{burst} = \Phi a_l d_{burst} \sigma_p + \Phi F_y A_s \quad \text{for radial direction} \quad (33)$$

$$T_{burst} = \Phi h_{anc} d_{burst} \sigma_p + \Phi F_y A_s \quad \text{for tangential direction} \quad (34)$$

The compressive stress under the jack shoes should also be compared to compressive strength of concrete. The compressive stress, can easily be calculated from the following equation:

$$\sigma_c = P_{pu} / a_l h_{anc} \quad (35)$$

ACI 544.7R-16 (2016) recommends the modification of compressive stress with Eq. (36) due to the fact that the pressure area does not cover all the surface.

$$f'_{co} = 0.85 f'_c \sqrt{\frac{a_t (h - 2e_{anc})}{a_l h_{anc}}} \quad (36)$$

It is also possible to calculate the bursting stresses with the analytical method of Iyengar diagram (ACI 544.7R-16, 2016). The ratio of bursting tensile stress ( $\sigma_{cx}$ ) to

compressive stress ( $\sigma_{cm} = F/ab$ ) is given for different depth values of the section as in Figure 2-23. If the capacity of the FRC section is not sufficient to withstand bursting stresses, the section may be reinforced with steel/FRP bars.

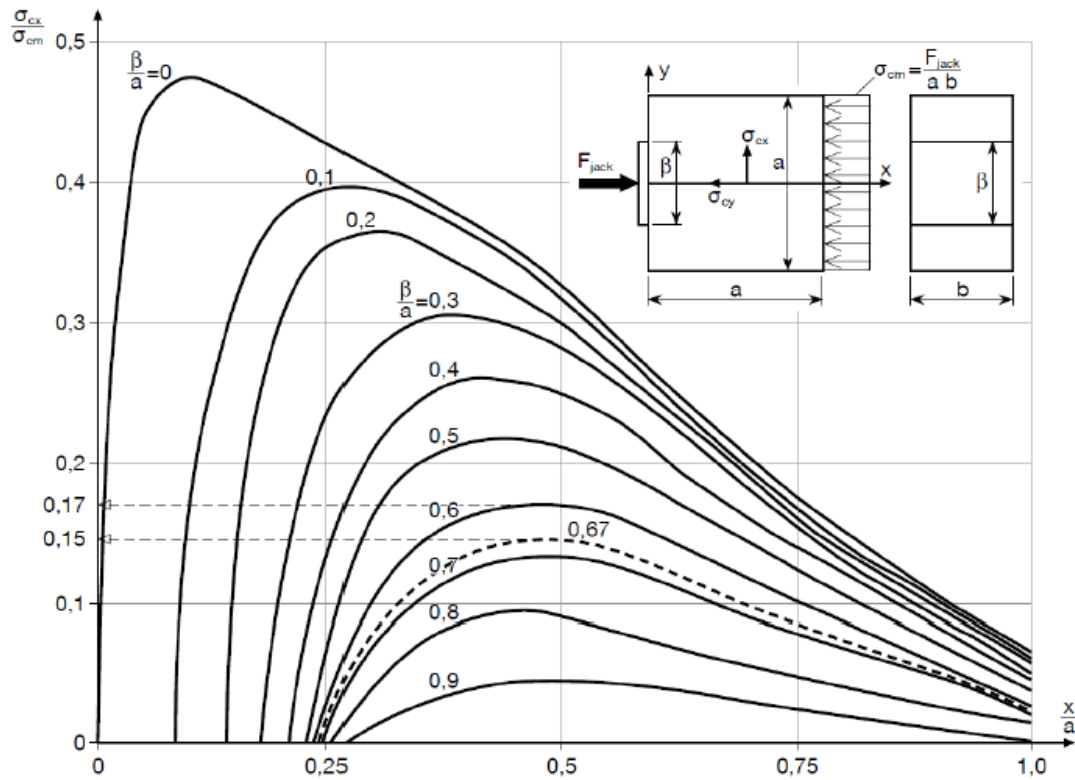


Figure 2-23 Iyengar Diagram for calculation of bursting stresses (ACI 544.7R-16, 2016)

There will be some voids between the precast linings and excavated soil. These voids will be filled with grouting. This loading case is called as tall skin back-grouting (ACI 544-7R-16, 2016). The developed forces are schematically shown in Figure 2-24. The equivalent specific weight of the grout can be determined by the following equation (Groeneweg 2007).

$$\frac{\pi}{4} D_e^2 b \rho_{eq} = \pi D_e h b \rho_{concrete} + 2 D_e b \tau_{yield} \quad (37)$$

The vertical component of the grout pressure can be determined by Eq. (38).

$$\Delta P_{g,invert} = p_{eq} + D_e \quad (38)$$

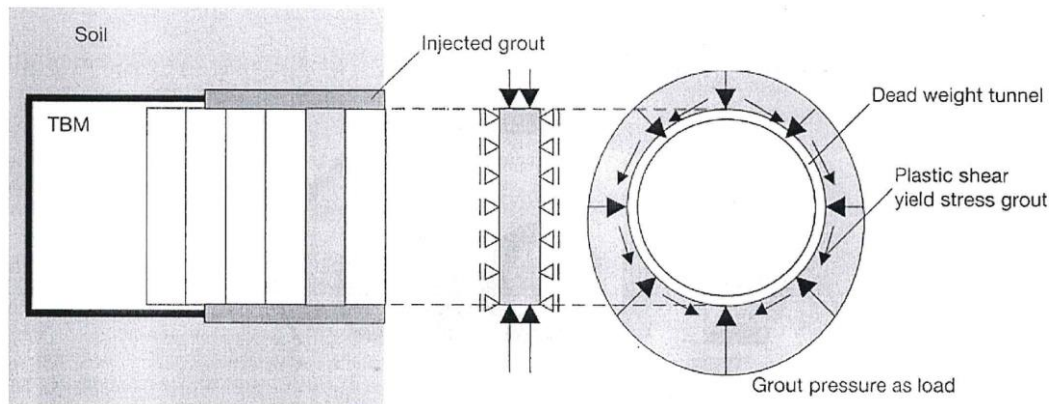


Figure 2-24 Schematic view of forces developed during tall-skin back grouting loading case (Groeneweg, 2007)

According to AASHTO DCRT-1 (2010) the maximum grout pressure is accepted as 69kpa above the groundwater pressure. However, the maximum pressure is taken as 150kpa above the groundwater pressure in South East Asia (Itatech Report no:22, 2019). Since there is no interaction between the ground and tunnel, the analysis is done with a FEM as a solid ring. The stiffness of the solid ring should be reduced because of the segment joints (Itatech Report no:22, 2019, ACI 544-7R-16, 2016). The self-weight of the segments and the grouting pressure should be applied as the loading cases. A load factor of 1.25 is recommended in ACI 544-7R-16 (2016) for both of the load cases. This load case may lead to significant axial force and bending moments in the section and should be checked by an axial-load moment interaction diagram (ACI 544-7R-16, 2016).

Secondary grouting is performed to fill the gaps with grout. The loading is schematically shown in Figure 2-25. The load case is defined in ITA WG2 (2000) and the force distribution is shown in Figure 2-26. Similarly, the stiffness in FEM should be decreased due to the presence of segmental joints. In this load case the segments are in contact with ground except where secondary grouting is applied (ACI 544-7R-16, 2016). Therefore, FEM should include the interaction between ground and precast tunnels. The interaction may be modelled with radial and tangential springs. The

stiffness of the springs may be determined from USACE EM 1110-2-2901 (1997). According to ACI 544-7R-16 (2016), this load case will result in high bending moments and low axial forces. Therefore, attention should be paid for this loading case.

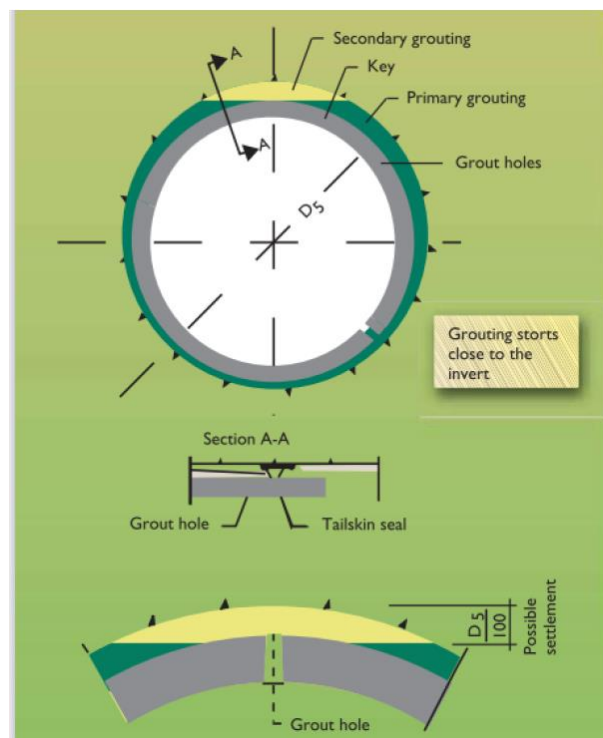


Figure 2-25 Secondary grouting (Guglielmetti et al. 2007)

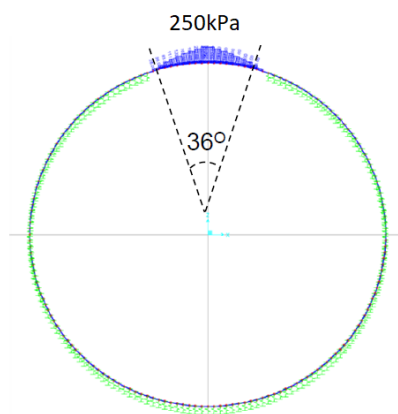


Figure 2-26 Secondary grouting pressure over one-tenth of the lining (grouting pressure value is indicative) (Itatech report no: 22, 2019)

Service load cases include earth pressure, groundwater and surcharge loads, longitudinal joint bursting load, loads induced due to additional distortion and other loads. Other loads may include seismic loads, fire loads explosion loads, breakouts at cross passageways, portals, shafts and excessive longitudinal bending moments. (ACI 544-7R-16, 2016).

The loads due to earth pressure, groundwater and surcharge loads may be analyzed by elastic equations, beam-spring models, FEMs and other methods reported in ACI 544-7R-16 (2016).

ITA WG2 (2000) proposed a simple method for the calculation of member forces for circular tunnels. The method does not require any FEM and based on the elastic equations. The method also includes the reduced bending rigidity due to the presence of segmental joints.

The beam spring method may be used as proposed by AASHTO DCRT-1, JSCE Tunnel engineering Committee (2007) and Austrian Society for Concrete and Construction Technology (2011). The method is similar to the one mentioned in secondary grouting procedure. The spring stiffness may be calculated with USACE EM 1110-2-2901 (1997).

The Austrian Society for Concrete and Construction technology (2011) and AFTES WG7 recommends using FEM method to calculate segment forces in soft ground, loose rock an partially homogenous rock. It is possible to model complex situations as well as non-uniform load distributions by the use of FEM techniques.

The load factors at ULS and SLS load cases are presented in Table 2-8. The capacity checks at SLS and ULS states should be performed upon calculation of the factored segment forces. It has been observed that, the industry uses a load factor of 1.5 in ULS calculations for all loading cases. Although there is not any numerical study, the approximation is found appropriate and conservative, because, when compared with Table 2-8 the maximum load factor given in the table, i.e., 1.5, is used for all loads.

However, the load combinations presented in Table 2-8 or combinations in EN 1990 (2002) may also be used in design calculations.

Table 2-8 Load factors for Service Loadings (ACI 544-7R-16, 2016)

Limit State	Self-weight, Groundwater pressure		Horizontal ground pressure, vertical ground pressure		Surcharge Load	
	Maximum	Minimum	Maximum	Minimum	Maximum	Minimum
ULS	1.25	0.90	1.35	0.90	1.50	0.75
SLS	1.0		1.0		1.0	

During the distribution of service load forces between the segments, the transfer may not be through full section. Besides, there may be some eccentricity during this transfer. Therefore, bursting stresses may occur in the precast segment during service loads. There are a number of methods to calculate the bursting stress developed in service stage. Some of these methods have already been mentioned previously, i.e., Iyengar Diagram, FEM models. The simplified equations may also be used for this load cases. According to ACI 544-7R-16 (2016), the German Tunneling Committee (2013) presents a more detailed approximation for the loading case. German Tunneling Committee (2013) proposes to have additional reinforcement for spalling stresses if the eccentricity of the loads is higher than  $d/6$ . The secondary stresses can be calculated with the following equations:

$$F_{sd} = 0.25 N_{ED} \left(1 - \frac{d_1}{d_s}\right) \quad (39)$$

$$F_{sd,r} = N_{ED} \left(\frac{e}{d} - \frac{1}{6}\right); F_{sd,2} = 0.3F_{sd,r} \quad (40)$$

The parameters are shown in Figure 2-27.

The capacity of the section can be determined by the equations that was presented for TBM thrust load cases. If the FRC's capacity is not enough to overcome the tensile stresses in the section, additional reinforcement can be added. The area of the reinforcement can be calculated by Eq. (33) and (34).

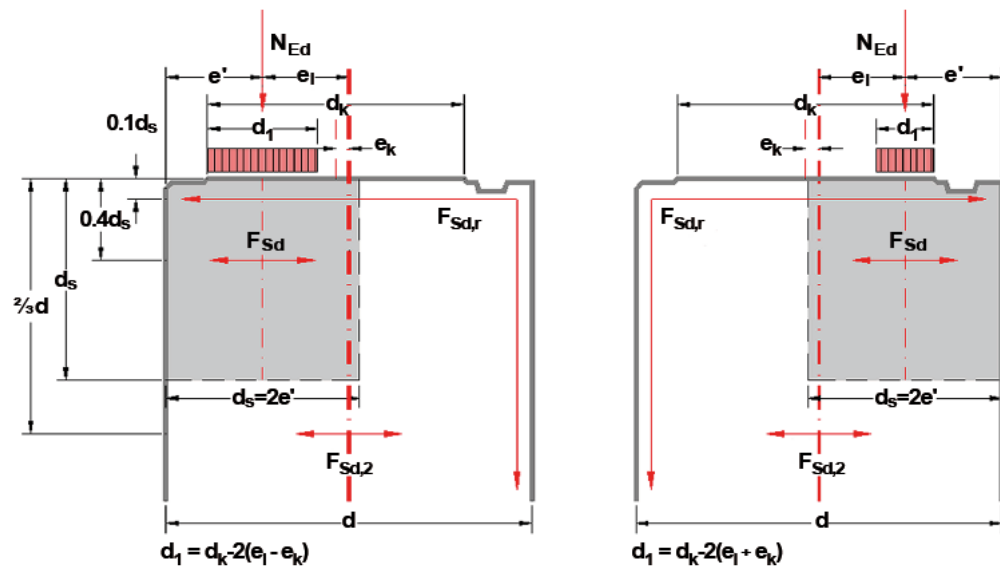


Figure 2-27 Precast Segment load transfer with eccentricity and formation of split tensile stress (Daub, 2013)



## CHAPTER 3

### DESIGN OF FRC TUNNEL SEGMENTS WITH FRP REINFORCEMENT

#### 3.1. Introduction

The design rules for FRC members and FRP reinforced concrete members are summarized in Chapter 2. Besides, additional design rules for precast tunnel segments including specific loading cases are also provided. A new and unique design methodology is presented in this chapter for FRC sections reinforced with FRP bars. In the first part, the design procedure at ULS is provided. The design rules at SLS are reviewed in the second part. The third part gives information regarding the mechanical criteria as defined in fib Model Code 2010 (2012) requirements. Finally, a recommendation for the calculation of shear capacity is provided.

#### 3.2. ULS Design

According to fib Model Code 2010 Bulletin 66 (2012), the bending failure is reached for FRC+RC members if one of the following conditions occurred:

- if the compressive strain is equal to the ultimate compressive strain
- if the tensile strain of steel is equal to the ultimate tensile strain of steel
- if the tensile strain of FRC is equal to ultimate tensile strain in FRC.

Similarly, For FRC precast segments reinforced with FRP bars, the bending failure may be occurred due to attainment of ultimate compressive strain or ultimate tensile strain of FRC or ultimate tensile strain of FRP reinforcement bars.

The maximum tensile strain for FRC members was defined in Eq. (14). For precast tunnel segments, the thickness of segments may vary between 20 cm to 60 cm according to the project requirements. Therefore, the maximum strain in FRC segments is calculated in between  $2.5/200 = 1.25\%$  and  $2.5/600 = 0.42\%$ .

The ultimate strain of FRP reinforcement may vary between 0.5% - 4.4%. As discussed in Chapter 2, the FRP reinforcement is accepted to have elastic behavior up to failure. If a material factor of  $\gamma_{FRP}=1.5$  and the environmental factor is applied to ultimate strain values, the design strain of FRP reinforcement will be between 0.3% - 2.9%. Therefore, the design may be controlled either by FRP rupture mode or by FRC ultimate tensile strain mode. If the tensile strain of FRC is reached before the ultimate design strain of FRP, the section capacity should be calculated according to the threshold of ultimate tensile strain of FRC. On the other hand, if the design tensile strain of FRP reinforcement is lower than the ultimate tensile strain of FRC, then the section capacity should be calculated according to the threshold of design tensile strain of FRP. The constitutive equations can be derived from Figure 3-1 & Figure 3-2.

In Figure 3-1 (b) & Figure 3-2 (b), the failure is due to the attainment of ultimate tensile strain of FRC. In this loading case the figures show that the concrete stress distribution is triangular. Actually, this may not be the case as the concrete strain may be very close to the ultimate compressive strain. For FRC concrete only, ACI 544.7R-16 (2016) shows triangular distribution for compressive stress at low axial loads, i.e. up to balanced failure. However, fib bulletin 83 (2017), recommends to use rectangular stress block both for compressive and tensional part of the section. Actually, as the width of the section for precast tunnel segments is considerably high, either of the stress distribution assumption gives similar result in terms of moment capacity of the section. For design purposes, two different stress distribution is taken for concrete in compression. If the maximum compressive strain value of the section is lower than  $\varepsilon_{c3}$ , i.e., 0.175%, for concrete class C50/60 or lower, triangular stress distribution is taken in calculations. On the other hand, if the maximum compressive strain is higher than  $\varepsilon_{c3}$ , rectangular stress block is assumed for compression.

Generally, for positive and negative moment values through the section, the reinforcement is placed in both inner side and outer side of the precast segments. However, the contribution of FRP reinforcement in compression should not be taken into account in design calculations as previously mentioned in Section 2.

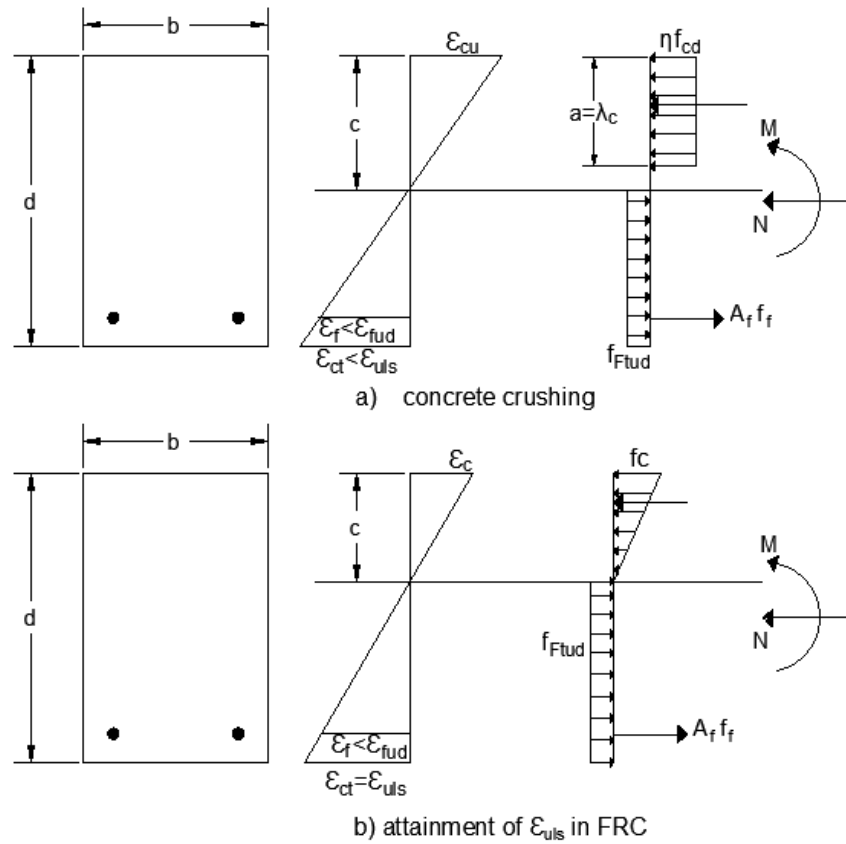


Figure 3-1 Strain- stress distributions in ULS for FRP + FRC sections (for sections with  $\epsilon_{uls} < \epsilon_{fu}$ )

As an example, a 300 mm thick tunnel segment with Glass Fiber Reinforced Polymer (GFRP) bar with an ultimate tensile strain of 2.0% is designed. The environmental factor for GFRP reinforcement is taken as 0.7 and the material factor,  $\gamma_{FRP}$ , is 1.5. Therefore, the design tensile strain of GFRP is  $2.0\% \cdot 0.7 / 1.5 = 0.93\%$ . According to fib Model 2010 (2012) the maximum tensile strain in FRC should be  $2.5 / 300 = 0.83\%$ . Therefore, the design will be controlled by maximum tensile strain in FRC.

As a second example, a 300mm thick tunnel with Carbon Fiber Reinforced Polymer (CFRP) reinforcement with an ultimate tensile strain 0.5% is designed. The environmental factor for CFRP reinforcement is taken as 0.9 and the material factor,  $\gamma_{FRP}$ , is 1.5. Therefore, the ultimate tensile strain of CFRP is  $0.5\% \cdot 0.9 / 1.5 = 0.3\%$ . According to fib Model Code (2012) the maximum tensile strain in FRC should be  $2.5 / 300 = 0.83\%$ . Therefore, the design is controlled by design tensile strain of CFRP.

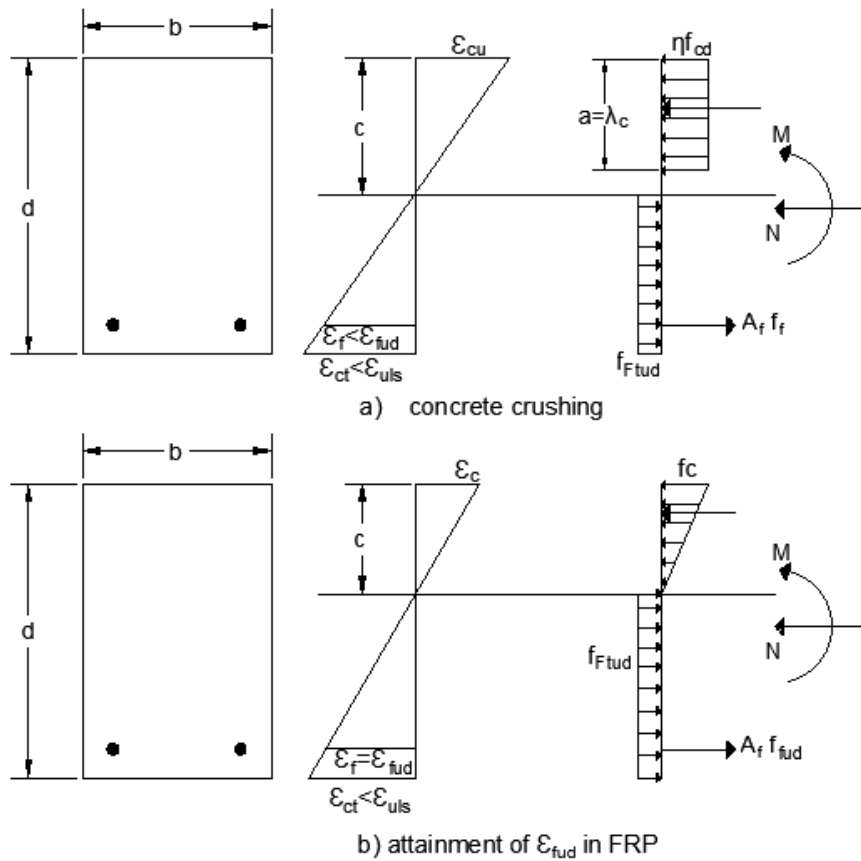


Figure 3-2 Strain- stress distributions at ULS for FRP+FRC sections (for sections with  $\epsilon_{uls} \geq \epsilon_{fu}$ )

It is possible to write a simple routine for the construction of axial load-moment (N-M) diagram at ULS with the compatibility equations derived from Figure 3-1 and Figure 3-2. A flowchart for such a routine is provided in Figure 3-3.

As a case study, consider a tunnel with 300mm wall thickness is to be built. The width of precast segments is 1500mm. According to fib Model Code 2010 (2012), the maximum tensile strain in FRC should be  $2.5/300 = 0.83\%$ . GFRP reinforcement with a rupture strain of 2.0% will be used as reinforcement. Design strain of FRP bars is calculated as  $C_E \epsilon_{FU}^* / \gamma_M = 0.7 * 2.0\% / 1.5 = 0.93\%$ . The concrete class is C40/50. The compressive design strength is calculated as  $f_{cd} = \alpha_{cc} f_{ck} / \gamma_c = 40 / 1.5 = 26.7$  MPa. Long term coefficient,  $\alpha_{cc}$ , is taken as one as proposed by fib bulletin 83 (2017). 4 $\phi$ 10 GFRP bars are used as tensile reinforcement. The rupture strength of FRP bars is taken as 895 MPa. The concrete cover is 40 mm. A residual strength value of  $f_{R3k} = 2.0$  MPa

is used in design. According to fib Model Code 2010 (2012), if rigid plastic approach is assumed, the tensile strength of concrete can be calculated as  $f_{Ftu} = f_{R3k} / 3 / \gamma_{ct} = 2.0 / 3 / 1.5 = 0.44$  MPa. The material factor is taken as 1.5 as recommended by fib Model Code 2010 (2012). A typical example of N-M envelope at ULS is shown in Figure 3-4 for the section discussed. Additionally, the N-M envelope for plain concrete and FRC section with same geometric and material properties are provided for reference.

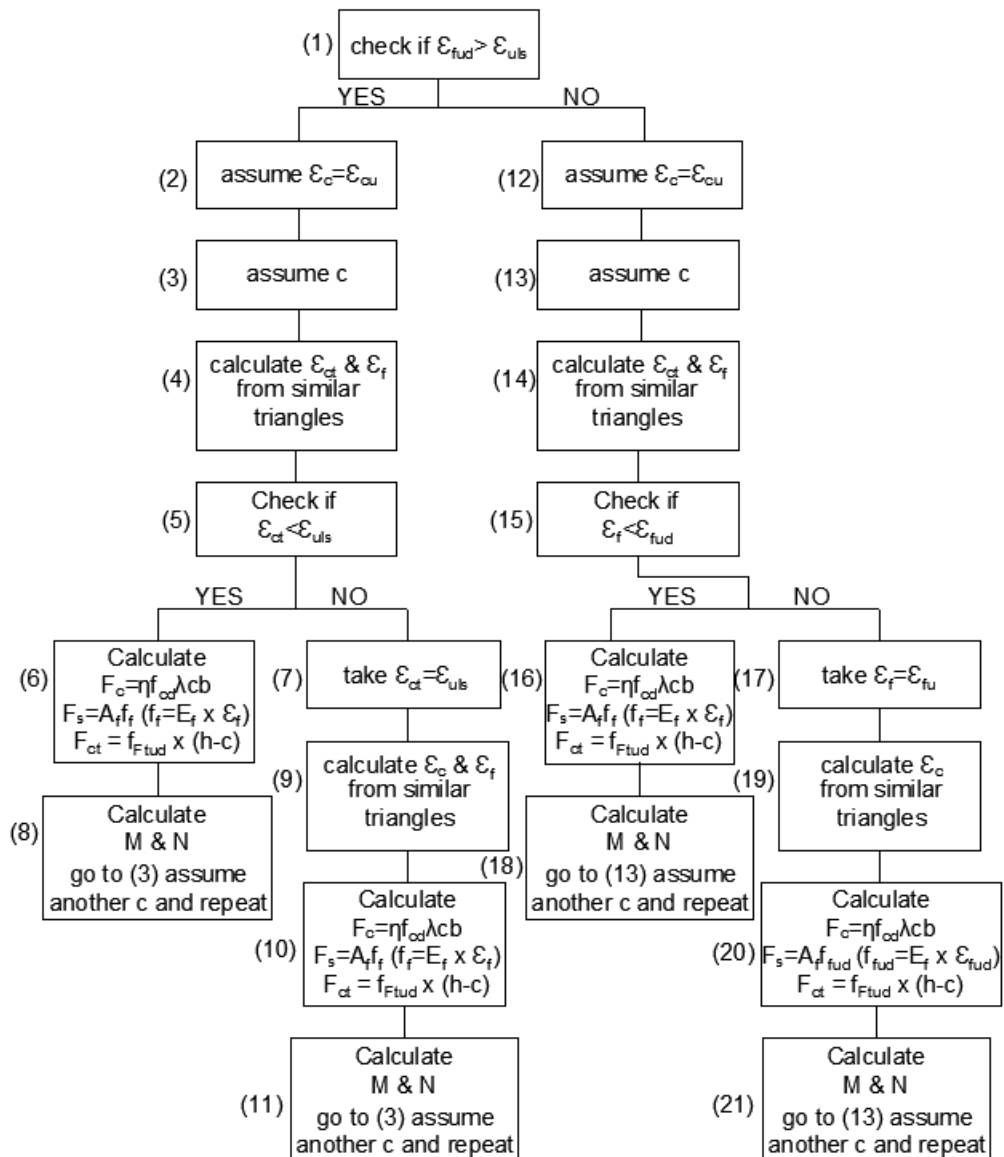


Figure 3-3 Flowchart for calculation of Moment Capacity of FRC+FRP at ULS

Alternatively, the section can be designed with FRC only with same geometric properties. If the concrete compressive strength is taken equal to the previous example, the same capacity can be achieved with  $f_{R3k} = 4.0$  MPa. The capacity of GFRP + FRC section with  $f_{R3k} = 2.0$  MPa is almost identical to FRC section with  $f_{R3k} = 4.0$  MPa as it is shown in Figure 3-5.

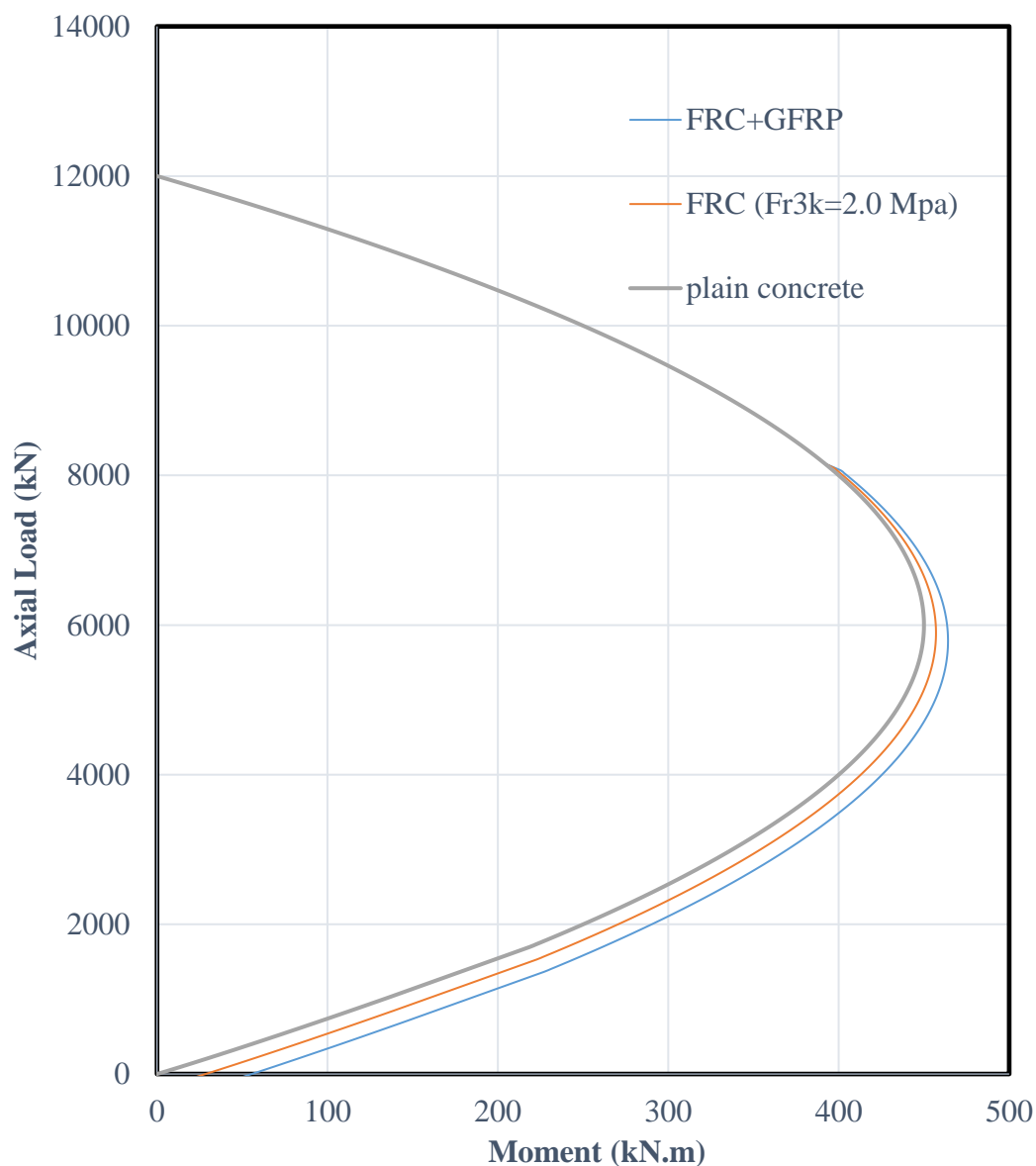


Figure 3-4 N-M Diagram for FRC + GFRP section ( $f_{R3k} = 2.0$  MPa) and FRC section ( $f_{R3k} = 2.0$  MPa)

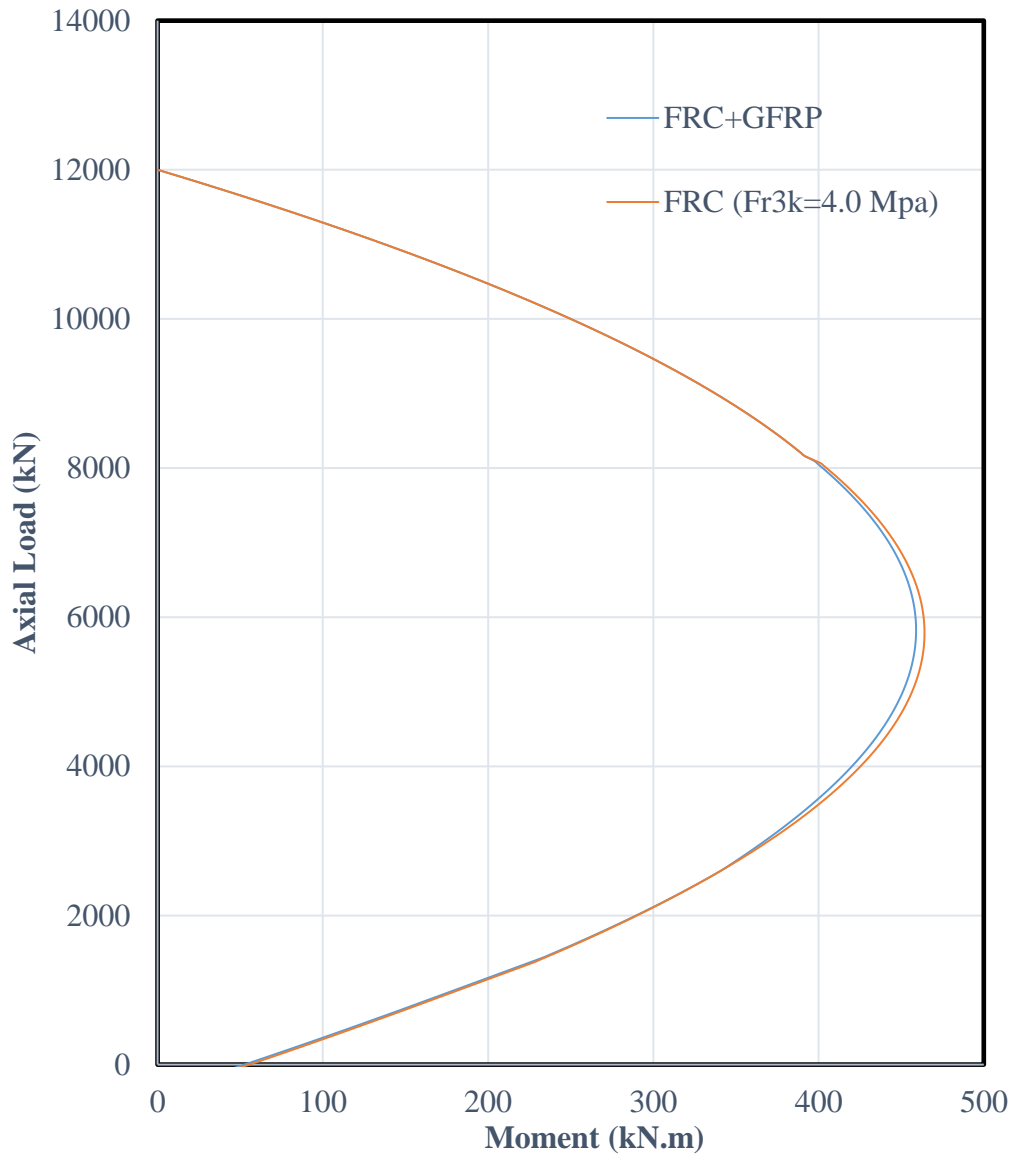


Figure 3-5 N-M Diagram for FRC + GFRP section ( $f_{R3k} = 2.0$  MPa) and FRC section ( $f_{R3k} = 4.0$  MPa)

### 3.3. SLS Design

At SLS, the crack width was limited to 0.3 mm as mentioned previously in Chapter 2 (Di Carlo et al., 2016). If the thickness of the precast members is assumed to be between 200 mm to 600 mm then the permitted strain can be calculated as,  $\epsilon_{sLS} = w/l_{CS} = 0$  to 0.15%. The threshold for FRP bars is due to the stress limitation of reinforcing bars, which should be between  $0.20f_{iuk}$  and  $0.8f_{iuk}$  at SLS. If the stress-strain

relationship of FRP bars is assumed to be linear elastic, then the SLS strain of FRP bars can be limited to  $0.20\varepsilon_{fu}-0.8\varepsilon_{fu}$ . Therefore, the strain limit for FRP bars at SLS is calculated as 0.1%- 3.2% including the environmental factor,  $C_E$ . As a result, the design at SLS is controlled with FRC tensile strain generally. The contribution of FRP bars can be added by the stress developed in bars.

The construction of axial load-moment diagrams at SLS is possible for the known crack width (Di Carlo et al. 2016).

As stated in Chapter 2, minimum crack width is required during transient loading cases. Therefore, Eq. (28) is also applicable for FRC reinforced with GFRP bars.

If required, further evaluation of crack width with FRP reinforced sections may be reviewed. It should be noted that, the crack width calculations might be revised to take into account the recommended reinforcement layout in precast segments. The proposed layout by Tiberti et al. (2008) is shown in Figure 3-6. The reinforcements are placed at the end zones of the linings and there is a wide space without reinforcement, for example, more than 700mm. Due to the discrete distribution, different crack patterns may be observed in the section. The residual strength parameters of FRC is important to control these crack patterns. Therefore, the residual strength limitations provided in Eq. (15) and Eq. (16) should be satisfied.

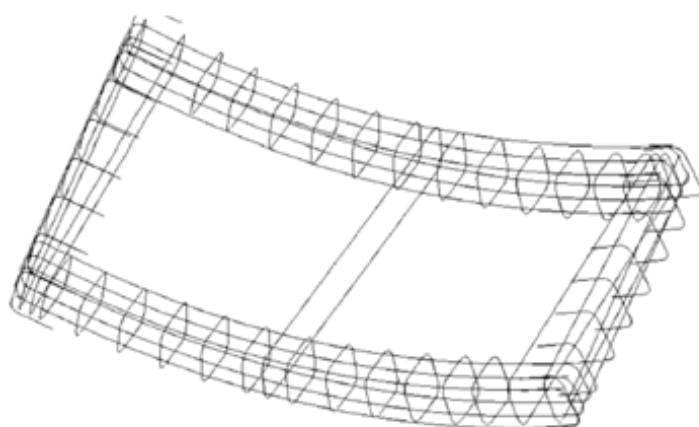


*Figure 3-6 Recommended reinforcement layout for precast tunnel linings (Tiberti et al. 2008)*

### 3.4. Mechanical Criteria

According to fib Model Code 2010 (2012), the following mechanical criteria should be satisfied.

- The ultimate load should be higher than the crack initiation load and Service Loads,  $P_u \geq P_{cr}$  and  $P_u \geq P_{SLS}$
- The ultimate vertical displacement should be higher larger than displacement at SLS level  $\delta_u \geq \delta_{cr}$
- The displacement at SLS should be 5 times lower than the maximum displacement  $\delta_{Peak} \geq 5 \delta_{SLS}$

In the first criteria, the load may be converted with moment, so that the moment capacity of the section must be higher than the cracking moment. i.e.,  $M_u \geq M_{cr}$  (L. Liao et al., 2015). According to fib bulletin 83 (2017), the criteria for displacement control need not to be checked for precast segments. The displacement criteria is imposed to have a minimum deformation capacity especially needed for indeterminate structures (fib bulletin 83, 2017). The segments will subject to bending moments during transient stages such as demoulding, storage, transport and handling. During these stages, generally, the segments have statically determinate support conditions (fib bulletin 83, 2017).

The ultimate design moment value,  $M_d$  can be read from the N-M envelope constructed for ULS design calculations. As the axial load is zero for transient stages, the corresponding moment can be taken as the ultimate moment.

According to fib bulletin 83 (2017) the cracking moment,  $M_{cr}$ , can be calculated with the equation below:

$$M_{cr} = \frac{b h^2}{6} f_{ctd,fl} \quad (41)$$

$f_{ctd,fl}$  = design flexural tensile strength

$$f_{ctd,fl} = f_{ctm,fl} / \gamma_{ct}$$

$f_{ctm,fl}$  can be calculated in accordance with EN 1992-1-1 (2004)

$$f_{ctm,fl} = \max \left\{ \left( 1.6 - \frac{h}{1000} \right) f_{ctm}; f_{ctm} \right\}$$

$h$  = total member depth in mm

$f_{ctm}$  = mean axial tensile strength, in accordance with EN 1992-1-1 (2004)

$\gamma_{ct}$  = partial safety factor for flexural tensile strength of concrete

$b$  = section width (mm)

$h$  = section height (mm)

If the same case study mentioned in Chapter 3.2,  $M_{cr}$  value would be calculated as follows:

For 300mm thick precast tunnels with a width of 1500mm which is built with C40/50 concrete,

$$M_{cr} = \frac{1500 \cdot 300^2}{6} \left\{ \left( 1.6 - \frac{300}{1000} \right) 3.5 \right\} / 1.5 * 10^{-6} = 68 \text{ kN.m}$$

The design moment value for zero axial value is taken from Figure 3-4.

$$M_d = 52 \text{ kN.m}$$

$$M_{cr} > M_d$$

The mechanical criteria is not satisfied. According to fib bulletin 83, this criteria may not be satisfied for FRC sections. If this criteria is not satisfied, then an additional partial factor for concrete is to be applied in design,  $\gamma_N = 1.20$ . The same procedure may be adopted for FRC sections reinforced with GFRP bars. The same additional factor should also be applied to GFRP reinforcement. The N-M diagrams, given previously, should be recalculated with the additional partial safety factor. The demand/capacity checks for both transient and permanent load cases should be done according to the N-M interaction diagram calculated with the additional partial factor. It is also recommended to perform full-scale testing for this kind of calculation

approach (fib bulletin 83, 2017). The full scale experiment test results provided in the following chapter shows that the ultimate capacity of the precast segments are higher than the cracking moment values.

### 3.5. Design Checks for Precast FRC Tunnel Segments reinforced with FRP

The loading conditions for precast linings were summarized in Chapter 2. The design values can be calculated similarly. However, there are some differences for calculation of capacity calculations in some of the loading cases.

The transient stage checks for both SLS and ULS cases can be performed with the previously mentioned methodology. The recommendation of Itatech Report no: 16 (2016) for the uncracked state check is also applicable for FRC+GFPR.

The bursting stresses that will be developed during the advance of TBM machine can be calculated similarly. Eq. (33) and Eq. (34) calculates the capacity of FRC sections reinforced with conventional reinforcement. However, a modification is required for FRC precast tunnel sections reinforced with FRP bars. The capacity calculations can be performed by considering the two cases for the design. If the tensile strain of FRC is reached before the ultimate design strain of FRP, the section capacity should be calculated according to the threshold of ultimate tensile strain of FRC. On the other hand, if the design tensile strain of FRP reinforcement is lower than the ultimate tensile strain of FRC, then the section capacity should be calculated according to the threshold of design tensile strain of FRP. For the first case, i.e.,  $\varepsilon_{uls} < \varepsilon_{fud}$ , Eq.(42), Eq.(43), Eq.(44) and Eq.(45) can be used for the capacity calculations.

$$T_{burst} = \Phi a_l d_{burst} \sigma_p + \Phi F_f A_f \quad \text{for radial direction} \quad (42)$$

$$T_{burst} = \Phi h_{anc} d_{burst} \sigma_p + \Phi F_f A_f \quad \text{for tangential direction} \quad (43)$$

Alternatively, if the fib Model Code design approach is adopted for concrete, the ACI 544 equations may be re-arranged as shown in Eq. (44) and Eq. (45).

$$T_{burst} = a_l d_{burst} F_{r3k} / \gamma_{ct} / 3 + f_f A_f \quad \text{for radial direction} \quad (44)$$

$$T_{burst} = h_{anc} d_{burst} F_{r3k} / \gamma_{ct} / 3 + f_f A_f \text{ for tangential direction} \quad (45)$$

For the second case, i.e.,  $\varepsilon_{uls} > \varepsilon_{fud}$ , Eq.(46) and Eq.(47) may be used.

$$T_{burst} = F_{fu} / \gamma_f A_f \text{ for radial direction} \quad (46)$$

$$T_{burst} = F_{fu} / \gamma_f A_f \text{ for tangential direction} \quad (47)$$

### **3.6. Shear capacity of FRC segments reinforced with FRP**

The shear capacity of FRP reinforced concrete sections was provided in Eq. (7). Besides, the shear capacity of FRC sections can be calculated with Eq. (27). As a conservative recommendation, the shear capacity of the FRC sections reinforced with FRP bars can be accepted as the minimum value calculated by these two equations until a more detailed research is conducted on this subject. Besides, the proposed equations is not verified with experiments yet.

## CHAPTER 4

### EXPERIMENTAL PROGRAM

#### 4.1. Introduction

İzmir F.Altay- Narlıdere subway project and İstanbul Ümraniye Ataşehir Göztepe projects are planned to be built as precast tunnel segments. The tunnel segments are designed to be macro-synthetic fibers concrete reinforced with GRRP bars as an alternative to traditionally reinforced segments. Small scale test for İzmir and full-scale tests for both İzmir and İstanbul are performed at METU structural laboratory.

#### 4.2. Test Specimens, Set-up and Material Properties

İzmir F.Altay- Narlıdere and İstanbul TBM tunnel is designed to have 5.7 m inside diameter. The thickness of the segments is 30cm. The length of the each precast element is 1.5 m. Rings consist of six segments. Five of the segments are parallelogram and one of them is trapezoidal. The angle of parallelogram segments is  $67.5^{\circ}$ . The key element has an angle of  $22.5^{\circ}$ . The isometric view and sectional details of TBM segments is shown in Figure 4-1. The section of view of the tunnels is provided in Figure 4-2. Full-scale tests are performed in one of the parallelogram segments. The average horizontal length of one segment is approximately 3.333 m on center. The curved length is 3.534 m on center. Approximate segment weight is 39.76 kN. The segments include  $4 \text{ kg/m}^3$  macro-synthetic fiber. The properties of macro-synthetics are provided in Table 4-1. Concrete class is selected as C45/55 for İzmir project. The concrete class for İstanbul project is C40/50. For İzmir project, cylinder test-specimens are taken from full-scale test member. The results are provided in Table 4-2. For İstanbul project, cylindrical test specimens are taken independently at the field and at concrete batch plant. The mean value of the test specimen is reported as 79.4 MPa.

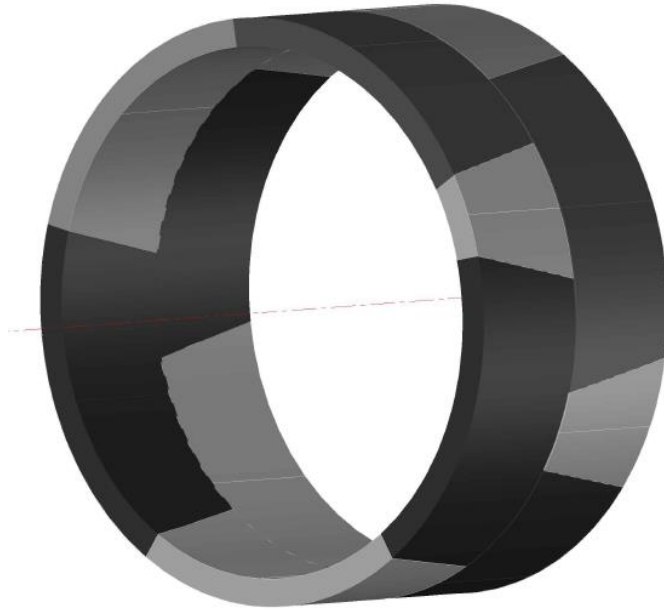


Figure 4-1 Isometric View of TBM rings

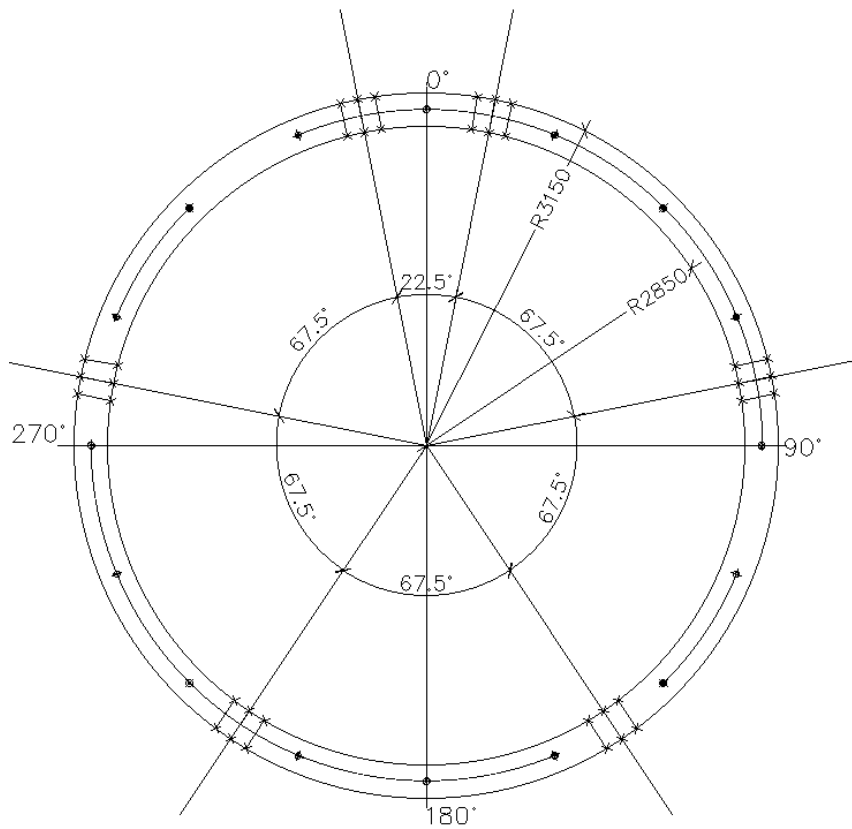


Figure 4-2 Section view of TBM tunnels

Table 4-1 *Macro-Synthetic fiber properties*

Type	Polypropylene
Length (mm)	54
Diameter (mm)	0.677
Aspect Ratio	79.76
Tensile Strength (MPa)	550-750
Elastic Modulus (MPa)	5750
Density (kg/m <sup>3</sup> )	910
Number of fiber per kg (approximate)	220000

Table 4-2 *Compressive strength values of test specimens taken from full-scale test member after bending test for İzmir Project*

No	Testing Specimen	Dimensions		Area (mm <sup>2</sup> )	H/D Ratio	Crushing Load (kN)	Concrete Strength (MPa)
		D(cm)	H(cm)				
1	Field	9.2	19.2	6648	2.09	323.2	48.6
2	Field	9.2	19.5	6648	2.12	320.6	48.2
3	Field	9.2	19.5	6648	2.12	348.5	52.4
4	METU	9.4	19.4	6940	2.06	335.6	48.4
5	METU	9.4	19.0	6940	2.02	399.7	57.6
6	METU	9.4	19.0	6940	2.02	312.0	45.0
7	METU	9.4	19.4	6940	2.06	348.3	50.2
						<b>Mean</b>	<b>50.05</b>
						<b>Standard Deviation</b>	<b>4.02</b>

Both in İstanbul and İzmir projects, same amount of GFRP bar reinforcement is provided. The mechanical properties of the GFRP reinforcement is tested by the manufacturer at Yıldız Technical University. Three different specimen are subjected to tensile testing. The rupture strength and the modulus of the elasticity of the specimens are recorded. The results are tabulated in Table 4-3. The concrete mixture includes 4kg/m<sup>3</sup> macro-synthetic fiber in both of the projects.

Table 4-3 GFRP mechanical Properties (taken from manufacturer test report)

No	Tensile Strength (MPa)	Tensile Strain*	Modulus of Elasticity (MPa)
1	992	2.32%	42816
2	961	2.09%	46001
3	1025	2.35%	43709
Mean	925	2.25%	44175
Standard Deviation	26.13	0.11%	-
Guaranteed Value per ACI 440.1R (2015)	846	1.91%	44175

\* Only the tensile strength and modulus of elasticity values were reported in the manufacturer’s material report. The strain values are calculated by dividing the tensile strength values to Modulus of Elasticity values.

Sectional GFRP reinforcement layout for one precast tunnel segment is shown in Figure 4-3.

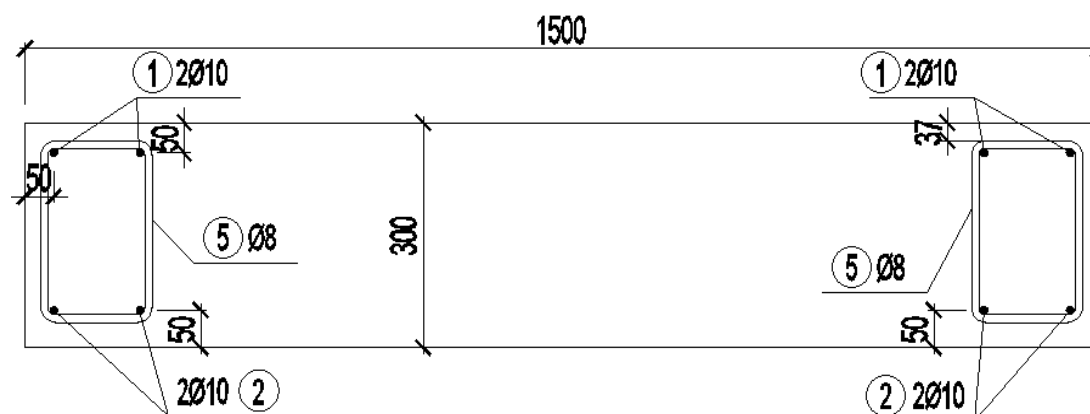


Figure 4-3 Sectional reinforcement layout for precast segments

The samples for determining the residual strength values are taken from the concrete mixture for İstanbul project. In order to determine the residual strength values of macro-synthetic fiber reinforced concrete, crack mouth-opening displacement (CMOD) versus load have been plotted as shown in Figure 4-4. The initial cracking strength and residual strength parameters are tabulated in Table 4-4 as previously mentioned in Chapter 2.3. The characteristic values are calculated in accordance with ITAtech report n.7 (2016).

Table 4-4 Beams test results according to EN 14651

No	l, Span length (mm)	b, Width (mm)	h (mm)	Residual Flexural Strength				
				F <sub>L0P</sub> (MPa)	F <sub>R1</sub> (MPa)	F <sub>R2</sub> (MPa)	F <sub>R3</sub> (MPa)	F <sub>R4</sub> (MPa)
1	500	155.0	147.5	6.43	1.71	1.96	1.88	1.64
2	500	152.0	147.5	5.85	1.03	1.19	1.15	1.02
3	500	155.0	152.5	6.08	0.97	1.07	1.01	0.89
4	500	152.0	147.5	7.41	1.29	1.55	1.47	1.23
5	500	153.0	147.5	6.96	1.36	1.50	1.38	1.19
6	500	152.0	150.0	6.04	0.71	0.76	0.74	0.64
7	500	155.0	150.0	6.43	1.74	2.04	1.90	1.63
8	500	155.0	150.0	6.80	1.04	1.16	1.16	1.08
9	500	150.0	149.0	6.92	0.96	1.05	0.98	0.86
10	500	152.0	151.0	6.70	1.50	1.66	1.61	1.39
11	500	150.0	150.0	6.66	1.33	1.50	1.43	1.27
12	500	152.0	150.0	6.55	1.42	1.67	1.57	1.40
13	500	150.0	150.0	6.87	1.47	1.79	1.71	1.47
14	500	150.0	150.0	7.35	1.25	1.40	1.36	1.30
15	500	153.0	150.0	7.00	1.24	1.45	1.37	1.17
16	500	155.0	150.0	6.86	1.19	1.26	1.18	1.03
17	500	155.0	150.0	7.16	1.38	1.56	1.47	1.24
18	500	152.0	150.0	6.74	1.32	1.52	1.45	1.23
19	500	153.0	150.0	7.15	1.45	1.70	1.63	1.40
20	500	155.0	149.5	6.98	1.26	1.37	1.25	1.16
21	500	153.0	150.0	6.45	1.30	1.46	1.33	1.17
22	500	152.0	150.0	6.74	1.64	1.88	1.82	1.70
23	500	152.0	150.0	6.00	1.31	1.49	1.42	1.30
24	500	152.0	151.0	6.46	1.14	1.29	1.26	1.08
25	500	151.0	150.0	5.82	1.57	1.85	1.72	1.50
26	500	154.0	150.0	6.68	1.52	1.71	1.63	1.38
27	500	153.0	150.0	6.75	1.22	1.39	1.38	1.20
28	500	150.0	150.0	6.13	1.02	1.16	1.16	1.06
29	500	152.0	149.0	6.50	1.27	1.45	1.38	1.22
30	500	153.0	150.0	6.38	1.33	1.51	1.43	1.26
Avg.	-	-	-	6.63	1.30	1.48	1.41	1.24
St. Dv.	-	-	-	0.41	0.23	0.28	0.26	0.23
COV%	-	-	-	6.2	17.6	19.1	18.8	18.5

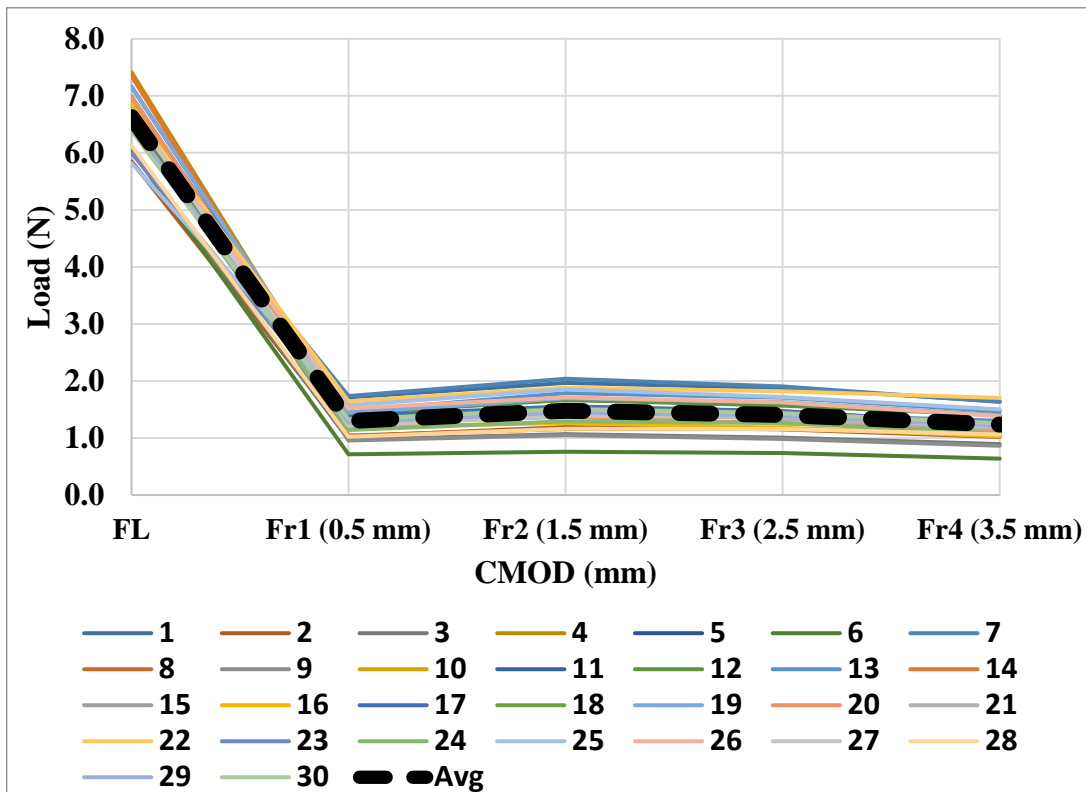


Figure 4-4 Load- CMOD curve for test beams in accordance with EN 14651

The mean of  $F_{LOP}$  is calculated as 6.63 MPa. The mean values of residual strength parameters is 1.30 MPa, 1.48 MPa, 1.41 MPa and 1.24 MPa respectively. Standard deviation is calculated for LOP as 0.41 MPa. The standard variation of residual strength parameters are 0.23 MPa, 0.28 MPa, 0.26 MPa and 0.23 MPa. The COV values for  $F_{LOP}$ ,  $f_{R1}$ ,  $f_{R2}$ ,  $f_{R3}$  and  $f_{R4}$  are calculated as 6.2%, 17.6%, 19.1%, 18.8%, and 18.5% respectively. According to ITAtech report no7 (2016), the maximum COV values for  $F_{LOP}$  and  $f_{R1}$  to  $f_{R4}$  values are recommend to be 15% and 25% respectively. Therefore, the test results are acceptable in terms of COV values.

The formulation for the calculation of characteristic strength is explained in section 2.3.1.

For crack control, the characteristic values can be calculated in accordance with ITAtech report no7 (2016). According to the report, for crack control, 95% reliable estimation of mean value may be used.

$$F_{LOPk} = 6.63 (1 - 0.00 * 0.062) = 6.63 \text{ MPa}$$

$$F_{RIk} = 1.30 (1 - 0.00 * 0.176) = 1.30 \text{ MPa}$$

$$F_{R2k} = 1.48 (1 - 0.00 * 0.191) = 1.48 \text{ MPa}$$

$$F_{R3k} = 1.41 (1 - 0.00 * 0.188) = 1.41 \text{ MPa}$$

$$F_{R4k} = 1.24 (1 - 0.00 * 0.185) = 1.24 \text{ MPa}$$

The same parameters for ULS design can be calculated as;

$$F_{LOPk} = 6.63 (1 - 1.64 * 0.062) = 5.95 \text{ MPa}$$

$$F_{RIk} = 1.30 (1 - 1.64 * 0.176) = 0.92 \text{ MPa}$$

$$F_{R2k} = 1.48 (1 - 1.64 * 0.191) = 1.01 \text{ MPa}$$

$$F_{R3k} = 1.41 (1 - 1.64 * 0.188) = 0.97 \text{ MPa}$$

$$F_{R4k} = 1.24 (1 - 1.64 * 0.185) = 0.86 \text{ MPa}$$

It is worth stating that the following condition is not satisfied for the sample:

$$F_{RIk} / F_{LOPk} > 0.4$$

Therefore, according to fib Model Code 2010 (2012), fiber reinforcement will not fully or partially substitute reinforcement at ultimate states. The minimum  $F_{RIk}$  and  $F_{R3k}$  to satisfy the requirements should be 2.38MPa and 1.19MPa respectively.

For İzmir project, five small scale beams are tested. The depth, width and length of beams were 200 mm, 300 mm and 1500 mm respectively. The reinforcement and fiber content details of the beams and the concrete cylinder test results for the beams are presented in Table 4-5. 7-days compressive strength of the specimens are recorded but the small-scale beam tests are performed at a later date than 28-days. So, in the last column of Table 4-5, the estimated 28-day compressive strength based on EN 1992-1-1 (2004) is presented.

Table 4-5 Small-scale test specimen mixture and material properties

No	Mixture	7-day Compressive Strength (MPa)	28-day Compressive Strength (MPa) (Calculated)
1	Plain Concrete	45.5	55.6
2	2 $\phi$ 10 Top and Bottom GFRP reinforcement	45.5	55.6
3	4kg/m <sup>3</sup> MSF	52.0	63
4	6kg/m <sup>3</sup> MSF	40.4	49.3
5	2 $\phi$ 10 Top and Bottom GFRP reinforcement + 4kg/m <sup>3</sup> MSF	52.0	63
			$f_{cm} = 57\text{MPa}$ $f_{ck} = 49\text{MPa}$

Full scale tests were previously performed by Tengilimoğlu (2019). The same test set-up is used for full-scale tests. The test set-up is shown in Figure 4-5.



Figure 4-5 Test setup for full scale bending test

The locations of LVDT' s and strain gauges in the full scale test member is shown in Figure 4-6.

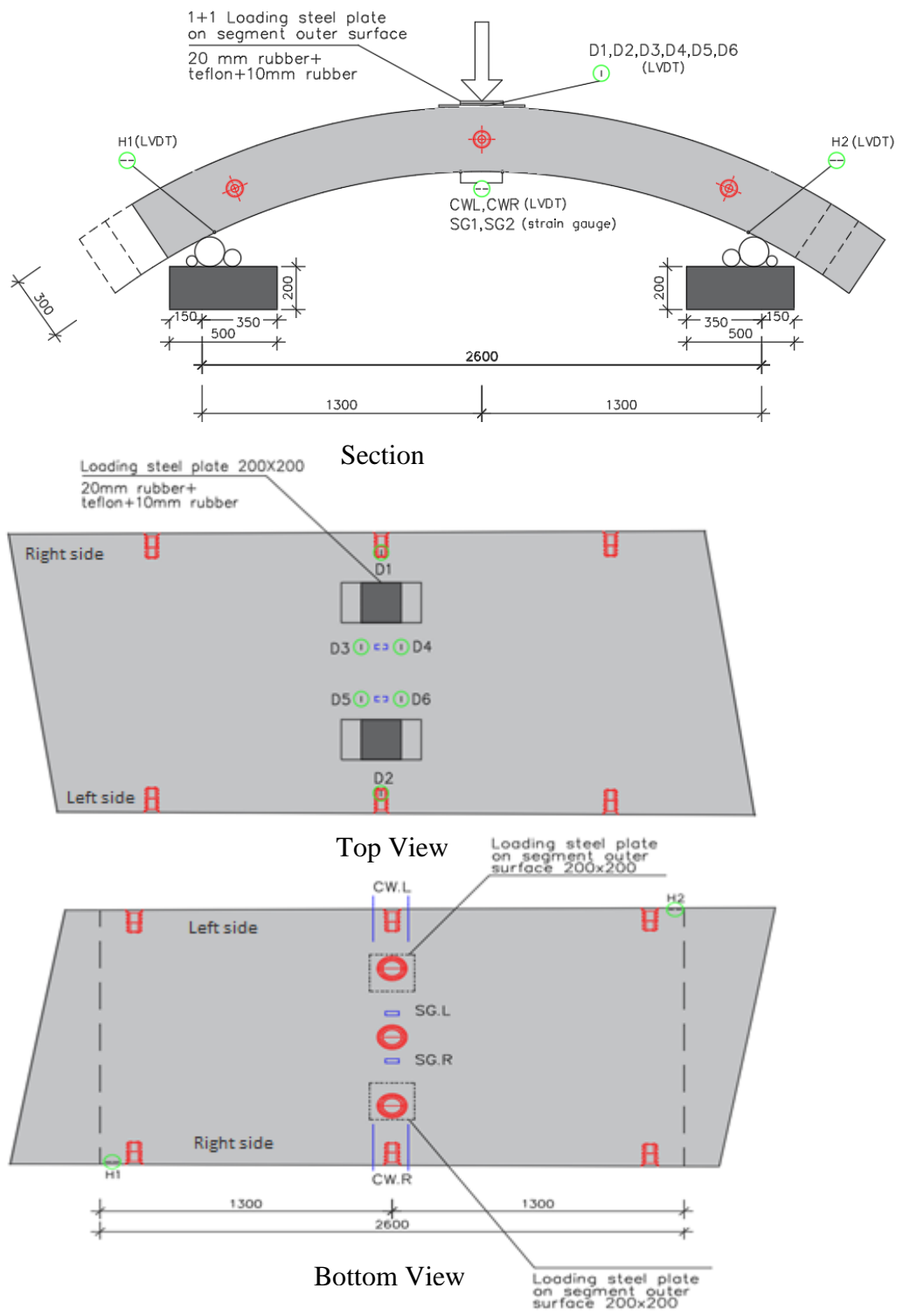


Figure 4-6 Locations of LVDT's and strain gauges in full scale test (Tengilimoğlu, 2019)

In addition to LVDT' s and strain gages that was used in Tengilimoğlu' s work (2019), two LVDT' s are attached to the top side of the specimen located on the maximum moment region, i.e., mid-span. The additional LVDT is connected to the specimen so that both tensional and compressive strains at the mid-span is recorded. As a result, the curvature is calculated and the moment curvature-diagram is plotted. The additional LVDT' s are added in one of the three full-scale tests. The location of the additional LVDT' s are shown in Figure 4-7.



*Figure 4-7* Additional LVDT' s to measure compressive and tensional strain of the specimen

The same test-up is also used for small-scale test specimens. The test-up for small scale tests is shown in Figure 4-8. The location of supports and the loading locations are shown in Figure 4-9. For 1.5m test specimen, the moment due to dead load is calculated as 0.4 kN.m. The moment due to applied force is calculated as  $P/2*0.4=P*0.2$ . The locations of the LVDT' s are shown in Figure 4-10. Totally five LVDT' s and one load cell are provided in the specimens. Two LVDT' s record the compressive strain, two LVDT' s record tensile strain and one LVDT records the vertical deflection.



Figure 4-8 Small scale test set-up

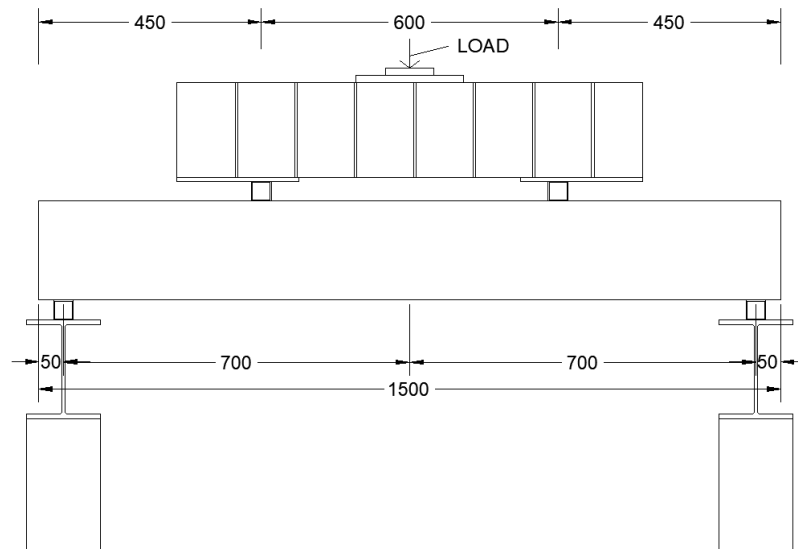


Figure 4-9 Small scale test specimen support and loading locations

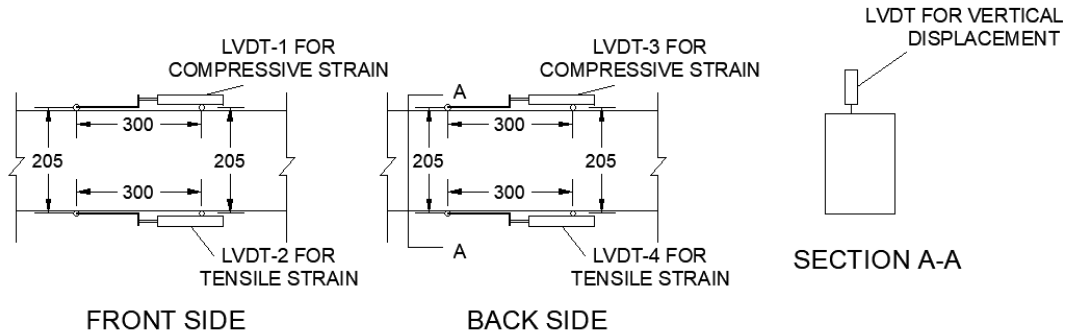


Figure 4-10 LVDT locations on small-scale test specimens

### 4.3. Full Scale Test Results

Three full-scale bending tests are performed for two different projects. The average vertical deflection has been measured at the mid-span by four LVDT's. The average of these four measurements has been taken and plotted versus applied load and illustrated in Figure 4-11. The cracking moments and the ultimate moment values can be calculated according to the test results. The moment due to dead load of the specimen is calculated as 9.25kN.m. The moment due to the applied load is  $0.65 \cdot P$ . The proposed method is used for the determination of ultimate moment capacity of the section. The capacity at 2.5 crack width is calculated. Therefore, the maximum allowed strain is  $2.5 \text{ mm} / \text{section depth (300mm)} = 0.83\%$ . All the material safety factors are taken as one for the estimation of ultimate value. The ultimate tensile strain of GFRP reinforcement is taken as 2.25%. If environmental factor,  $C_E$ , is applied to ultimate tensile strain, the maximum strain in the GFRP is calculated as  $0.7 \cdot 2.25\% = 1.58\%$ . The modulus of elasticity of the GFRP bars is taken as 43709 MPa in accordance with test results provided in Table 4-3. As the ultimate tensile strain of GFRP is higher than FRC's, the design is controlled by FRC ultimate tensile strain. Residual strength parameter,  $F_{R3}$ , is taken as the mean of the sample as provided in Table 4-4, which is 1.41 MPa. For İzmir Project, the mean compressive strength of concrete is used in calculations, which is 50 MPa. For İstanbul project same material properties is used in calculations with the exception of compressive strength of

concrete. The mean compressive strength of concrete is 79.4 MPa for İstanbul project. The Experimental and calculated moment values are summarized in Table 4-6.

Table 4-6 Cracking Moment and Ultimate Moment values for full-scale bending tests

Test Name	M <sub>cr</sub> (Cracking Moment) (kN.m)-experimental	M <sub>u</sub> (Ultimate Moment) (kN.m)-experimental	M <sub>u</sub> (Calculated by proposed method)
İstanbul	71.9	83.9	54.9
İzmir 01	56.5	68.3	54.7
İzmir 02	57.6	58.0	54.7

According to the results of the full scale test, the proposed method estimates the experiment results conservatively. In other words, the ultimate moment capacity of the section is higher than the calculated by the proposed method.

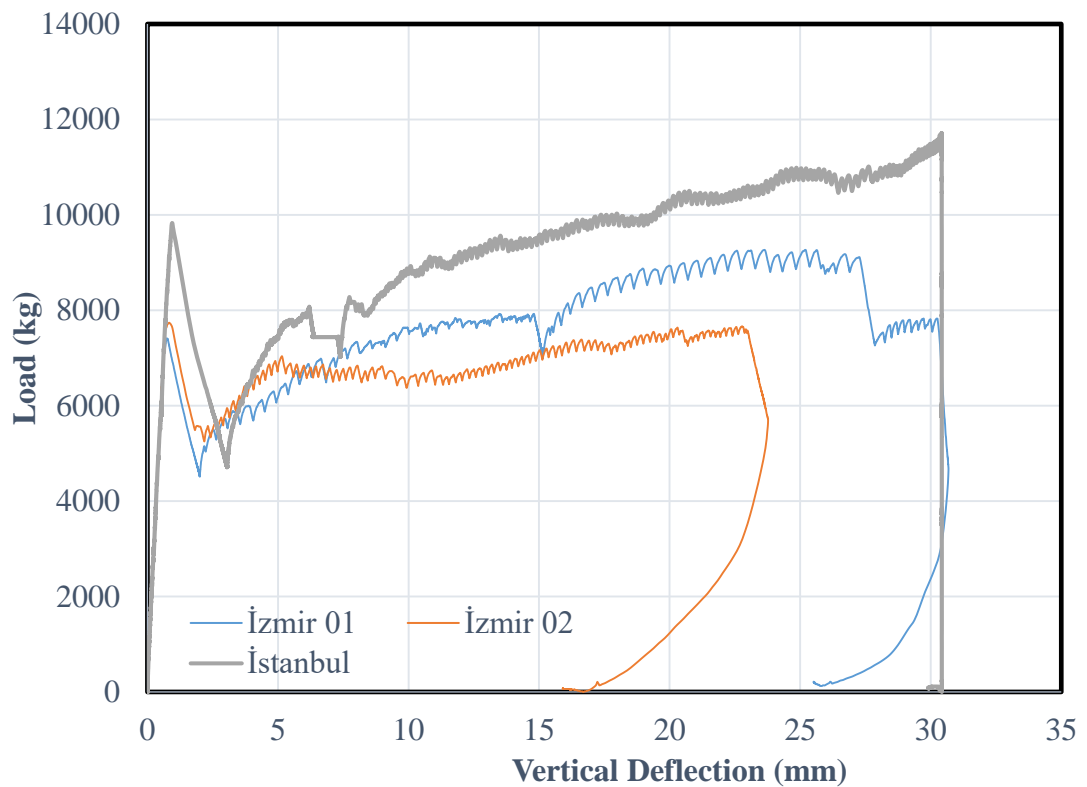


Figure 4-11 Load Deflection for full-scale bending tests

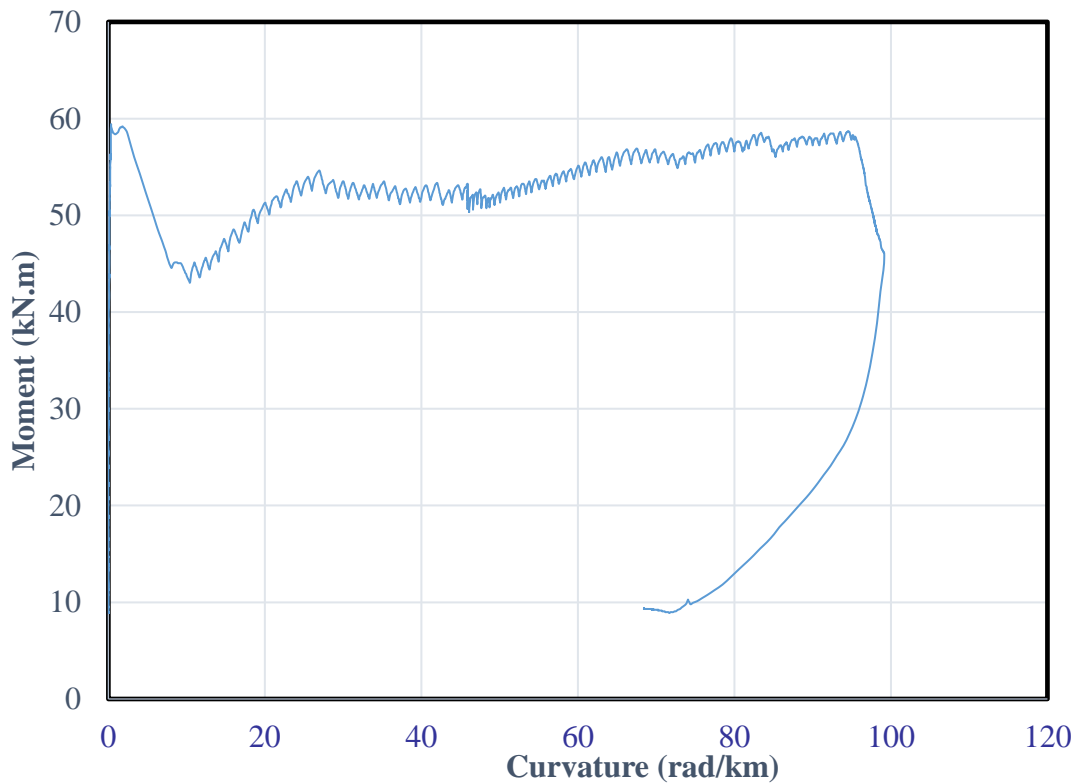


Figure 4-12 Moment Curvature Diagram for full-scale bending test, İzmir Project

#### 4.4. Small Scale Test Results

As previously stated, the vertical deflection of the small scale test specimen are measured by an LVDT. Figure 4-13 shows the P-vertical deflection for all of the test specimens. As it is observed from the results, there is no significant difference in the cracking moment of the test specimens as expected. This may be better observed in Figure 4-14. The cracking moments and the corresponding cracking stresses are tabulated in Table 4-7. According to the test results, there is no residual strength for 4 kg/m<sup>3</sup> SynFRC specimen. The beam showed brittle behavior during testing. No crack is observed during testing prior to splitting of the specimen. Actually, the testing was not deformation controlled however, deformation controlled test result was not satisfying as well. The results of the deformation-controlled tests may be observed in Table 4-4. Even if the results are for another project, as the material properties of synthetic fibers are same, same post-cracking results may be expected for these

members. Besides, the test results for 6 kg/m<sup>3</sup> mixture is not satisfactory. Small-scale test beams do not have a mouth opening however, as can be followed from Figure 4-13, the residual load after the first crack is 1000 kg maximum. If the same formulation given in EN 14651, i.e., Eq. (8), is used to determine the residual strength parameter;

$$f_{LOP} = \frac{3 * 45000 * 1400}{2 * 300 * 200^2} = 7.87MPa$$

$$f_{Res} = \frac{3 * 10000 * 1400}{2 * 300 * 200^2} = 1.75MPa$$

Therefore, the ductility criteria given in fib Model Code 2010 (2012) and ACI 544-7R (2016) is not satisfied for 4kg/m<sup>3</sup> and 6kg/m<sup>3</sup> SynFRC. The ultimate moment capacities of the beams are summarized in Table 4-8. The theoretical values are calculated considering;

- The ultimate strain of GFRP bars is 2.25%
- The modulus of elasticity of GFRP bars is 43709 MPa
- The concrete compressive strength is 50 MPa
- The residual strength of SynFRC is taken as  $F_{R3} = 1.41MPa$
- Material safety factors and environmental factor for GFRP bars concrete and FRC are taken as one for the estimation of experimental results

For small-scale test of GFRP+FRC section, the reinforcement ratio was much higher than the full-scale test. According to the proposed method, the ultimate tensile strain was limited to  $2.5 / h = 1.25\%$ . However, the ultimate tensile strain of FRP bars have not been reached. As the load carrying capacity of FRP bars are considerably high compared to full scale test due to increased reinforcement ratio, the capacity of the section is not calculated accurately, i.e., approximately half of the experimental value. This may be better understood with the specimen with GFRP reinforcement only. As can be followed from the results, the capacity of section is in accordance with the experimental values. However, for design calculations, the ultimate strain of GFRP

reinforcement will be divided by material safety factors or strength reduction factors. For example, if ACI 440.1R (2015) factors are applied, the ultimate strain will be limited to  $2.25 \% * 0.7 * 0.55 = 0.86\%$ . So, with the proposed method, the capacity of the GFRP reinforcement is subjected to a primary strength reduction factor, which is the ultimate tensile strain of FRC. As a result, the capacity of the section is calculated much lower than the experimental results.

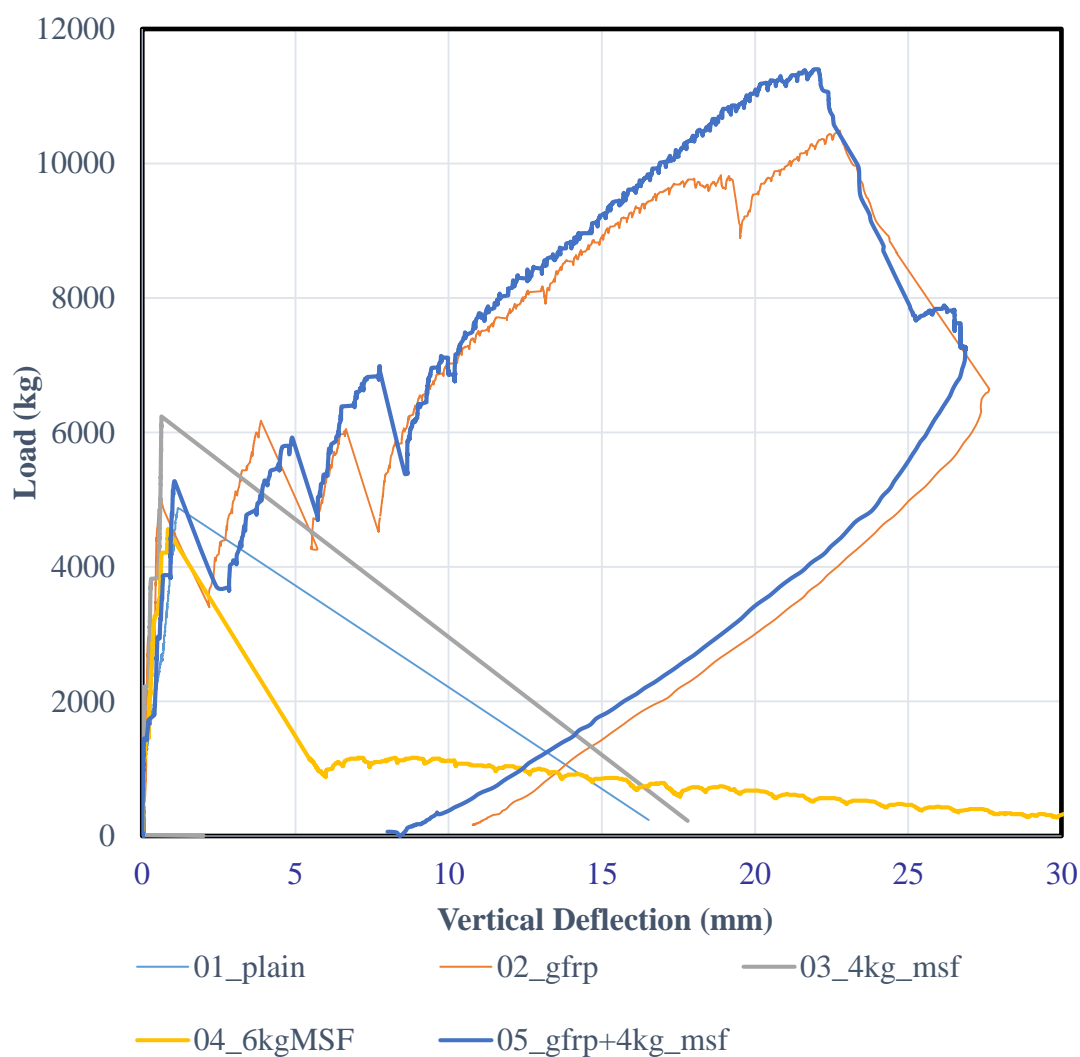


Figure 4-13 Load Deflection for small-scale bending tests

Table 4-7 Cracking moment and stresses for test specimens

No	Mixture	Cracking Load $P_{cr}$ (kg)	Cracking Moment $M_{cr}$ (kN.m)	Cracking Stress of Concrete $\sigma_{cr}$ (MPa)
1	Plain Concrete	4900	10.2	5.10
2	2 $\phi$ 10 Top and Bottom GFRP reinforcement	5000	10.4	5.20
3	4kg/m <sup>3</sup> MSF	6250	12.9	6.45
4	6kg/m <sup>3</sup> MSF	4500	9.4	4.70
5	2 $\phi$ 10 Top and Bottom GFRP reinforcement + 4 kg/m <sup>3</sup> MSF	5250	10.9	5.45

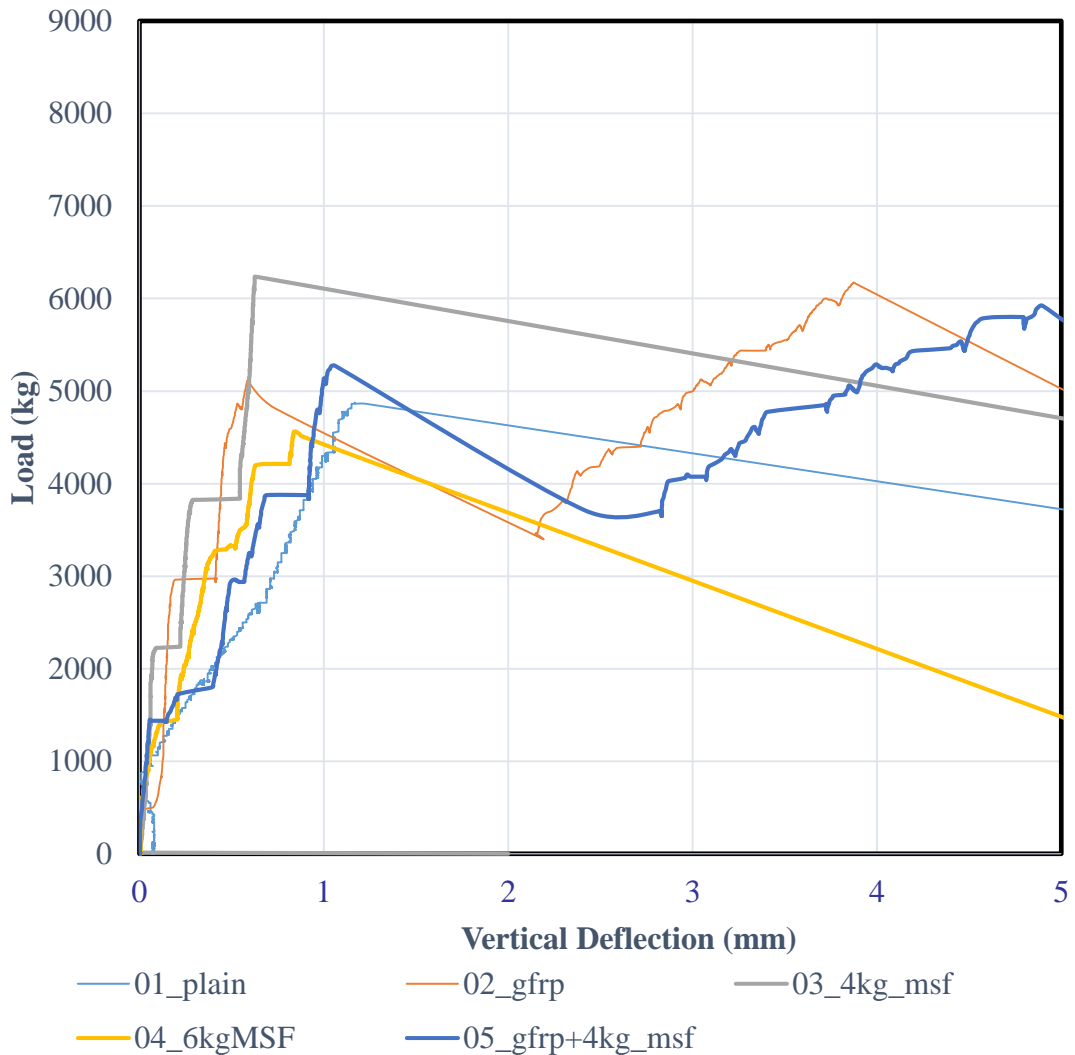


Figure 4-14 Load Deflection for small-scale bending tests, zoomed for cracking load

Table 4-8 Ultimate Moment Capacities for Test-Specimen

No	Mixture	Ultimate Load $P_u$ (kg)	Maximum Moment $M_U$ (experimental) (kN.m)	Ultimate Moment $M_U$ (teorotical) (kN.m)	Notes
1	Plain Concrete	4900	10.2	-	-
2	2 $\phi$ 10 Top & Bottom GFRP reinforcement	10487	21.38	23.1	Calculated in accordance with ACI 440 (2015)
3	4kg/m3 MSF	6250	12.9	-	-
4	6kg/m3 MSF	4500	9.4	-	-
5	2 $\phi$ 10 Top & Bottom GFRP reinforcement + 4kg/m3 MSF	11400	23.2	12.5	Calculated in accordance with the proposed method in Chapter 3.

Another important observation from the test results is the local load drops for beams including GFRP. The number of drops are equal to the number of cracks developed in concrete beams. Theses cracks may be observed in Figure 4-15 and Figure 4-16. The reason of these load drops is may be because of the poor bonding characteristics of FRP bars with concrete. Moreover, the pattern of cracks show similar behavior for RC section reinforced with plain bars.



Figure 4-15 Location of cracks for Test beam -2 before failure

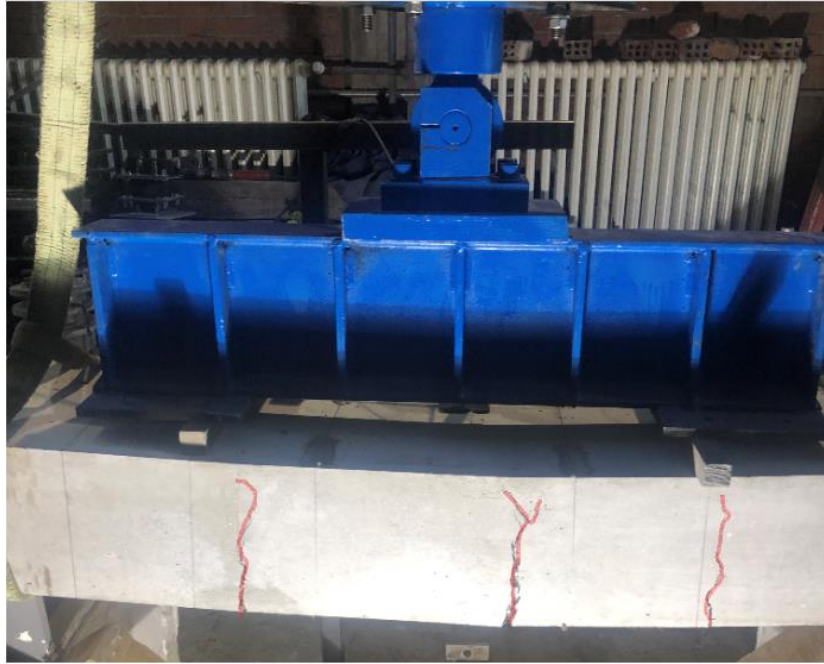


*Figure 4-16* Location of cracks for Test beam -5 before failure

As mentioned previously, the compressive and the tensile strain of the test-specimens are measured. However, in order not to harm the testing devices, the LVDT's measuring the top and bottom displacements have been removed from the specimens after 1.0% tensile strain at the bottom most fiber of FRC. Up to that strain level, the moment curvature of the specimens is shown in Figure 4-17. According to the results, the contribution of SynFRC is observed both in P-Deflection and in M-Curvature diagrams. As expected, the behavior up to first cracking is almost identical however, after the formation of first crack, the behavior starts to change. The results also show that, the material parameters for GFRP are in accordance with the expected values as the capacity of the section is calculated accurately for GFRP reinforced section. The number of tests should be increased so that, the verification of the proposed method would be further achieved. Furthermore, the proposed method is not taking into account the contribution of FRC at ultimate tensile strain of GFRP. By conducting repetitious tests with different material and geometric properties, it is possible to develop a more accurate method for determination of ultimate capacity.

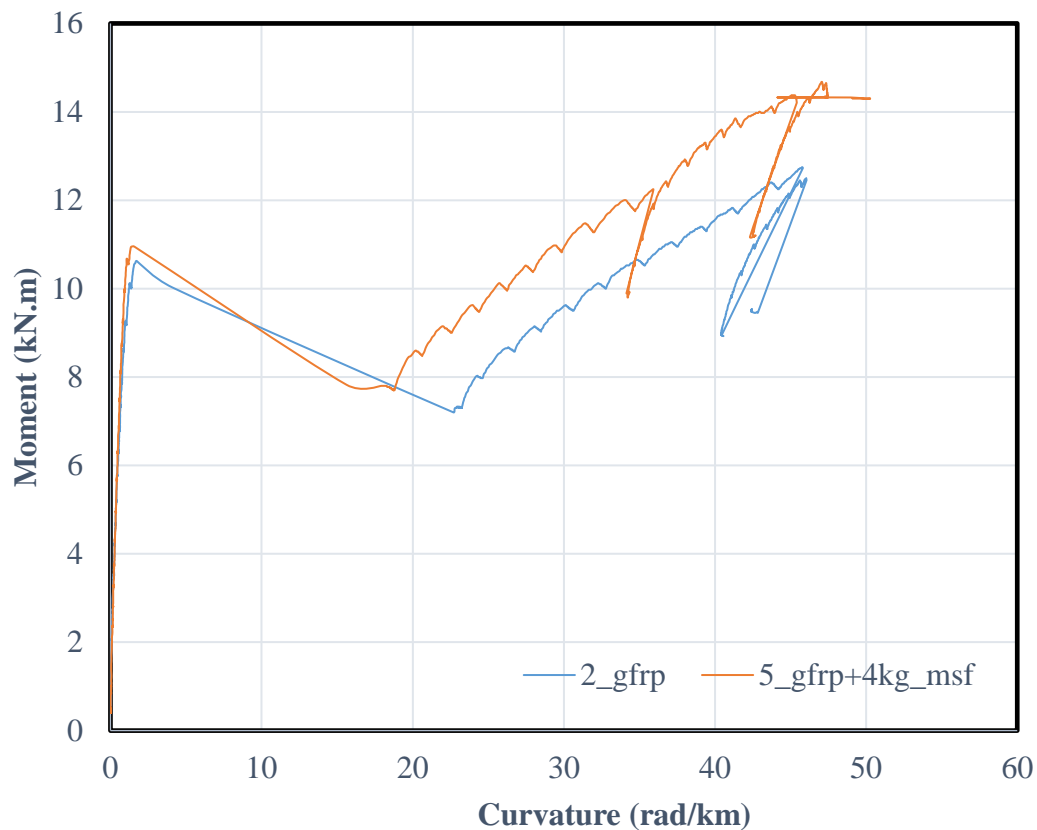


Figure 4-17 Moment-Curvature Diagram for small test specimen

According to the results of the experiments, it is not possible to satisfy the minimum criteria defined in design guidelines for FRC with  $4 \text{ kg/m}^3$  synthetic fiber. The small scale tests showed that there is no ductility in the specimen with  $4 \text{ kg/m}^3$  macro-synthetic fiber. Indeed, it is not a usual result when compared to other tests. The main reason of the brittle behavior is may be because of the poor mixture of macro-synthetic fibers during concrete mix. The specimen with  $6 \text{ kg/m}^3$  fiber showed some ductility. However, it is not satisfying the minimum requirements mentioned previously. The specimen with GFRP bars showed similar behavior with reinforced concrete sections with plain bars. The number of observed cracks are lower than conventional reinforced concrete sections with deformed bars. Besides, the crack widths of specimen with GFRP is considerably high when compared to conventional RC sections. The FRC specimen with GFRP bars showed similar behavior with the specimen with GFRP bars. The crack widths and the formation of the cracks are

similar. If load deflection curves and moment curvature curves are reviewed together, it is possible to state that SynFRC effected the behavior positively at SLS and ULS levels. However, the effect is not found to be satisfactory in terms of capacity as the increase in capacity in both of the levels are considerably low.



## CHAPTER 5

### CONCLUSIONS

In this thesis, an analytical procedure for FRP reinforced SynFRC tunnel segments is developed. The procedure is similar to the existing design guidelines/design codes. However, due to the difference in behavior of FRP bars, some modifications are introduced in the design methodology.

The existing design rules/methods are reviewed for both FRP reinforced concrete members and FRC members. The additional design rules/checks for precast tunnel segments is also checked. The design rules at SLS and ULS cases are reviewed for both of the FRC and FRP reinforced members.

Experimental studies are also performed in order to check the reliability of the proposed methodology. Due to the difference in tensile strain capacities of FRC and FRP bars, the proposed method is taking the minimum of the two as the design threshold. This leads to a “pre-defined safety coefficient” for FRP bars in design calculations. Further experiments should be performed in order to verify the behavior at ultimate limit state. The behavior at ULS should be documented for a number of specimen with different material and geometrical properties. So that, it will be possible to develop a better approximation at SLS and ULS.

The results of the experiments show that SynFRC residual strength parameters are not adequate in the tested specimen. The residual parameters should be increased so that the minimum code requirements and the capacity calculations should be verified. It should also be stated that, these parameters have great importance when the axial load on the segments are considerably low. The axial loads on segments can be neglected during transient stages, i.e., demoulding, storage, transportation and handling. During the service time, the segments will have bending moment with high axial loads.

Therefore, the capacity of the section, during service time of the tunnel, will slightly be affected by the residual strength parameters of the SynFRC.

The residual strength parameters of FRC will also effect the crack growth, which may be occurred during transient stages or TBM advance stage. Low residual strength values will lead to wider cracks developed in the precast members.

According to the small-scale and full-scale experimental results, the mechanical properties of the GFRP bars are in accordance with the previously mentioned values. In small scale tests, the GFRP reinforcement ratio is considerably high when compared to full-scale test results. This results in a higher ultimate moment capacity than expected. According to the small scale results, SynFRC effected the ultimate capacity positively. However, the contribution of SynFRC was very limited due to poor residual strength parameters.

It is also concluded that, the mixture of SynFRC in concrete mix plays a crucial role in residual strength parameters. In small scale tests, some of the beam specimen broke suddenly as it is in plain concrete.

This thesis is mainly dealt with analytical solutions and the experimental results of SynFRC precast tunnel segments reinforced with FRP bars. The future studies may include;

- Additional small scale and full scale tests with varying FRP reinforcement ratios and macro-synthetic fiber content
- Additional experiments to check the given formulation about shear capacity of the segments containing FRP and macro-synthetic FRC
- Fire behavior of precast segments made of FRC and FRP. It is recommended that, the fire behavior and load carrying capacity during the fire event and after the fire should be analyzed.
- Long-term behavior of precast segments under sustained loads should be analyzed.

## REFERENCES

- AASHTO DCRT-1-2010 (2010) Technical Manual for design and construction of road tunnels- Civil elements
- ACI Committee 440 (2015). ACI 440.1R-15. Guide for the design and construction of structural concrete reinforced with fiber-reinforced polymer (FRP) bars. 11 p.
- ACI Committee 544 (2016). ACI 544.7R-16 Report on design and construction of fiber-reinforced precast concrete tunnel segments
- ACI Committee 544 (2016). ACI 544.8R-16 Report on indirect method to obtain stress-strain response of fiber-reinforced concrete (FRC)
- Allmendinger, R. W., Cardozo, N. C., and Fisher, D., 2013. Structural Geology Algorithms: Vectors & Tensors: Cambridge, England, Cambridge University Press, 289 p.
- Caratelli, A. Meda, A. Rinaldi, Z. Spagnuolo, S., Maddaluno G. (2017). Optimization of GFRP reinforcement in precast segments for metro tunnel lining. Composite Structures 181, 336-346 1 p.
- Caratelli, A. Meda, A. Rinaldi, Z. Spagnuolo, S. (2016). Precast tunnel segments with GFRP reinforcement 1 p.
- CNR DT 203/2006 (2006). Guidelines for the design and construction of concrete Structures reinforced with Fiber-Reinforced Polymer Bars, Italian National Research Council
- Daub German Tunnelling Committee (Deutcher Ausschuss für unterirdisches Bauen e.V.) (2013). Recommendations for the design, production and installation of segmental rings.
- Di Carlo, F., Meda, A., Rinaldi Z., (2016) Design procedure for precast fibre-reinforced concrete segments in tunnel lining construction. Structural Concrete 17, No.5
- EN 1990:2002 (2002) Basis of Structural design. European Standard
- EN 1992-1-1. (2004). Design of concrete structures- Part 1-1: General rules and rules for buildings. European Standard
- EN 14651. (2005) Test method for metallic fibered concrete- measuring the flexural tensile strength. European Standard
- fib bulletins 40 (2007). FRP reinforcement in RC structures: Technical report. International Federation for Structural Concrete

- fib bulletins 65 (2012). Model Code 2010: Final Draft Volume 1. International Federation for Structural Concrete
- fib bulletins 66 (2012). Model Code 2010: Final Draft Volume 2. International Federation for Structural Concrete
- fib bulletin 83 (2017). Precast tunnel segments in fibre-reinforced concrete. State-of-the-art report fib WP 1.4.1.
- German Tunneling Comitee, 2013, "Lining Segment Design: Recommendations for the design, production and installation of Segmental Rings,"Taschebuch für den tunnelbau, Ernst und Sohn, Berlin, pp. 17-121.
- Groeneweg, T., (2007) Shield driven tunnels in ultra-high strength concrete: reduction of the tunnel lining thickness. Msc thesis, Delft University of Technology, the Netherlands.
- Guglielmetti, V., Grasso, P., Mahtab, A., Xu, S., (2007) Mechanized Tunneling in Urban Areas: Design Methodology and Construction Control CRC Press, 528 pp.
- ITATech report No 7 (2016). Itatech design guidance for precast fiber-reinforced segments- vol 1: design aspects. April 2016, pp. 47, ISBN 978-2-9701013-2-1.
- ITATech report No 16 (2016). Twenty years of FRC tunnel segments practice: lessons learnt and proposed design principles. April 2016, pp. 71, ISBN 978-2-9701013-5-2
- ITATech report No 22 (2019). Guidelines for the design of segmental tunnel linings. April 2019, ISBN 978-2-9701242-1-4
- ITA WG2 (2000). Guidelines for the Design of shield tunnel lining, Tunneling and Underground Space Technology, 15 (3): 303-331
- Liao, L., Fuente, A., Cavalaro, S., Aguado, A., Cabonari, G., 2015. Experimental and analytical study of concrete blocks subjected to concentrated loads with an application to TBM-constructed tunnels. Tunneling and underground space technology 49, 295-306
- Liao, L., Fuente, A., Cavalaro, S., Aguado, A., (2015). Design of FRC tunnel segments considering the ductility requirements of the Model Code 2010. Tunneling and Underground Space Technology 47, 200-210.
- Meda, A., Rinaldi Z., Caratelli A., Cignitti F., (2016). Experimental investigation on precast tunnel segments under TBM thrust action, Engineering structures 119, 174-185.
- RILEM TC 162-TDF (2003): Test and design methods for steel fiber reinforced concrete,  $\sigma$ - $\varepsilon$  design method. Materials and Structures, 36, 560-567.

- Tengilimođlu, O. (2019). An experimental study to investigate the possibility of using macro-synthetic fibers in precast tunnel segments (Master thesis, Middle East Technical University, Ankara, Turkey).
- Tiberti, G., Plizzari, G.A., Walraven, J.C., Blom, C.B.M., (2008) Concrete tunnel segments with combine traditional and fiber reinforcement. Tailor Made Concrete Structures- Walraven&Stoelhorst (eds) 2008 Taylor & Francis Group, ISBN 978-0-415-47535-8.
- U.S. Army Corps of Engineers (USACE) EM 1110-2-2901 (1997) Tunnels and shafts in Rock